Atmos. Chem. Phys. Discuss., 15, 34091–34147, 2015
www.atmos-chem-phys-discuss.net/15/34091/2015/
doi:10.5194/acpd-15-34091-2015


Atmospheric Chemistry and Physics Discussions



# Modeling lightning-$NO_x$ chemistry at sub-grid scale in a global chemical transport model

**A. Gressent[1], B. Sauvage[1], D. Cariolle[2,3], M. Evans[4,5], M. Leriche[1], C. Mari[1], and V. Thouret[1]**

[1]LA, CNRS, Université Paul Sabatier III de Toulouse, Toulouse, France
[2]Météo France, Toulouse, France
[3]Centre Européen de Recherche et de Formation Avancée en Calcul Scientifique, CERFACS, Toulouse, France
[4]Wolfson Atmospheric Chemistry Laboratories (WACL), Department of Chemistry, University of York, York, YO10 5DD, UK
[5]National Centre for Atmospheric Science (NCAS), University of York, York, YO10 5DD, UK

Received: 20 October 2015 – Accepted: 17 November 2015 – Published: 4 December 2015

Correspondence to: A. Gressent (alicia.gressent@aero.obs-mip.fr)

Published by Copernicus Publications on behalf of the European Geosciences Union.



## Abstract

For the first time, a plume-in-grid approach is implemented in a chemical transport model (CTM) to parameterize the effects of the non-linear reactions occurring within high concentrated $NO_x$ plumes from lightning $NO_x$ emissions ($LNO_x$) in the upper troposphere. It is characterized by a set of parameters including the plume lifetime, the effective reaction rate constant related to $NO_x$-$O_3$ chemical interactions and the fractions of $NO_x$ conversion into $HNO_3$ within the plume. Parameter estimates were made using the DSMACC chemical box model, simple plume dispersion simulations and the mesoscale 3-D Meso-NH model. In order to assess the impact of the $LNO_x$ plume approach on the $NO_x$ and $O_3$ distributions at large scale, simulations for the year 2006 were performed using the GEOS-Chem global model with a horizontal resolution of $2^\circ \times 2.5^\circ$. The implementation of the $LNO_x$ parameterization implies $NO_x$ and $O_3$ decrease at large scale over the region characterized by a strong lightning activity (up to 25 and 8 %, respectively, over Central Africa in July) and a relative increase downwind of $LNO_x$ emissions (up to 18 and 2 % for $NO_x$ and $O_3$, respectively, in July) are derived. The calculated variability of $NO_x$ and $O_3$ mixing ratios around the mean value according to the known uncertainties on the parameter estimates is maximum over continental tropical regions with $\Delta NO_x$ [−33.1; +29.7] ppt and $\Delta O_3$ [−1.56; +2.16] ppb, in January, and $\Delta NO_x$ [−14.3; +21] ppt and $\Delta O_3$ [−1.18; +1.93] ppb, in July, mainly depending on the determination of the diffusion properties of the atmosphere and the initial NO mixing ratio injected by lightning. This approach allows (i) to reproduce a more realistic lightning $NO_x$ chemistry leading to better $NO_x$ and $O_3$ distributions at the large scale and (ii) focus on other improvements to reduce remaining uncertainties from processes related to $NO_x$ chemistry in CTM.

## 1 Introduction

Lightning emissions are one of the most important sources of nitrogen oxides ($NO_x \equiv NO + NO_2$) in the upper troposphere (WMO, 1999; Hudman et al., 2007). Lightning emitted $NO_x$ ($LNO_x$) impact the tropospheric ozone burden (Stockwell et al., 1999; Hauglustaine et al., 2001; Grewe, 2007), and the hydroxyl-radical (OH) concentrations influencing the oxidizing capacity of the atmosphere (Labrador et al., 2004; Banerjee et al., 2014). Lightning flashes including cloud-to-ground and intra-cloud flashes produce reactive nitrogen species which are detrained in the cloud anvil (Weiss et al., 2012) and released directly in the upper troposphere. Because of an ozone production efficiency (OPE) 4 to 20 times larger in the upper troposphere than in the middle or low troposphere (Sauvage et al., 2007a; Martin et al., 2007), effects of $LNO_x$ on chemistry are expected to be stronger in the upper troposphere (Pickering et al., 1990; Hauglustaine et al., 1994; Zhang et al., 2003; Choi et al., 2009). The longer $NO_x$ lifetime in the upper troposphere (1–2 weeks) allows the long-range transport of $LNO_x$ through the large circulation patterns (Hemispheric Transport of Air Pollution, HTAP report, 2010: http://www.htap.org/).

Although the importance of the $LNO_x$ emissions on the upper tropospheric chemistry is well known, it remains highly uncertain with a best estimate of 2–8 $Tg\,N\,yr^{-1}$ (Schumann and Huntrieser, 2007). Lightning $NO_x$ emissions are associated with deep convection (horizontal scale $\sim 10$ km) and correspond to the "sub-grid" in global chemical transport models (horizontal resolution hundreds of kilometers). This implies that the impact of the lightning $NO_x$ emissions should be parameterized for inclusion into a large scale model. Global models commonly used convection proxies such as the cloud-top-height (Price and Rind, 1992) and the updraft intensity to estimate the lightning flashes. Flashes simulated by CTMs are commonly constrained by satellite observations (Sauvage et al., 2007b; Murray et al., 2012) such as measurements from the space-borne Lightning Imaging Sensor (LIS) and the Optical Transient Detector (OTD) on TRMM (Christian et al., 2003; Tost et al., 2007). The lightning $NO_x$ emissions are



then redistributed according to a vertical profile generally a "C-Shape" profile (Pickering et al., 1998) a priori defined depending on season, latitude and continent/ocean location. Also, corrections on the calculations of lightning $NO_x$ emissions using satellite observations (SCIAMACHY, Martin et al., 2007) and in-situ measurements (INTEX-NA, Hudman et al., 2007) are usually applied.

Despite the success in simulating the lightning $NO_x$ emissions, the small scale nature of the flashes and the non-linear chemistry (Lin et al., 1988) of the atmosphere will lead to biases on the large scale with instantaneous dilution of gases in the large grid box volume. It seems likely that this will lead to an overestimate of the OPE and an underestimate of the nitric acid ($HNO_3$) production. For instance, by forcing $NO_x$ concentration in GEOS-Chem grid box over Southeast Asia to represent the measured lightning plumes, Cooper et al. (2014) estimate a ratio for $O_3$ to $HNO_3$ produced leading to a 15 $mol\,mol^{-1}$ OPE in lightning plumes, that reinforces the fact that instantaneous dilution in global model implies issues in sub-grid chemistry.

In this work, a realistic lightning $NO_x$ chemistry as well as a plume parameterization is implemented into a global chemical transport model (CTM) allowing reproducing more accurately the large scale $NO_x$ and $O_3$ distributions. The plume approach used in this study was previously developed by Cariole et al. (2009) for aircraft $NO_x$ emissions in the LMDz-INCA and MOBIDIC models and also implemented to deal with the ship $NO_x$ emissions (Huszar et al., 2010). This approach avoids the double count in the CTM calculation of the emitted $NO_x$, first instantaneously diluted into the point grid and second as the plume form. In addition, the plume parameterization is the first that considers the $NO_x$ from lightning as a plume with the transport of the related non-linear chemistry effects. $NO_x$ from lightning emissions are emitted in the upper troposphere characterized by strong winds that allows large scale transport of trace species. Thus, it is relevant to consider a plume growth from lightning emissions, which could be diluted long time after the initial lightning pulse, downwind of emissions. Consequently, the plume parameterization previously developed for aircraft exhausts has been adjusted

to $LNO_x$ emissions and implemented into the GEOS-Chem global chemical transport model.

Section 2 gives a description of the GEOS-Chem model in which the plume-in-grid parameterization is implemented and models used to evaluate the diffusion properties of the atmosphere and to determine parameters characterizing the physics and chemistry of the lightning $NO_x$ plume. A concise description of the plume approach is then presented in Sect. 3 followed by a detailed explanation of the determination of parameters related to $LNO_x$ emissions. Section 4 summarizes the results of the simulations performed with GEOS-Chem and finally these results and the sensitivity on $NO_x$ and $O_3$ variations of the parameterization are discussed in Sect. 5.

## 2 Models

Three different models are used in this evaluation and are described in this section. GEOS-Chem is used to provide a global framework to assess the impact of lightning $NO_x$. Meso-NH is used to provide estimates of the plume diffusion timescales and DSMACC is a box model used to assess the non-linear chemistry in the plume.

### 2.1 The GEOS-Chem chemical transport model

The GEOS-Chem chemical transport model (Bey et al., 2001) is a global 3-D model of atmospheric composition driven by assimilated meteorology from the Goddard Earth Observing System (GEOS-5) of the NASA Global Modeling Assimilation Office (GMAO). The 09-01-01 version (http://wiki.seas.harvard.edu/geos-chem/index.php/GEOS-Chem_v9-01-01) of the CTM has been used in this study. The model transports 43 tracers to describe tropospheric $O_3$-$NO_x$-VOC chemistry. The horizontal resolution is $2^\circ \times 2.5^\circ$ and 47 vertical levels are defined from the ground to 80 km altitude. The CTM includes modules for emissions, transport, chemistry, deposition, aerosols and surface.



The large-scale advection of tracers is performed using the TPCORE advection scheme (Lin and Rood, 1996) corresponding to a semi-lagrangian flux method. Shallow and deep moist convection processes are carried out using the Relaxed Arakawa–Schubert scheme (Moorthi and Suarez, 1991). Mixing in the lower atmospheric layers is represented by a non-local scheme of the planetary boundary layer described by Lin and McElroy (2010). The wet deposition for water-soluble aerosols and for gases follows Liu et al. (2001) and Amos et al. (2012). Aerosol scavenging by ice crystals and cold/mixed precipitation is also reproduced in the model (Wang et al., 2011). The dry deposition is associated to a scheme which calculates bulk surface resistance in series (Wesely, 1989). Photolysis rates are calculated with the Fast-JX code (Bian and Prather, 2002). The atmospheric chemistry is resolved using the SMVGEAR solver (Jacobson and Turco, 1994) with more than 300 species and 785 chemical reactions. Heterogeneous chemical reactions are represented on the surface of the sulfate aerosols (Bey et al., 2001) and mineral dust (Martin et al., 2002). Effects of aerosols on the photolysis rates are based on Martin et al. (2003). Primary $NO_x$ and VOCs (Volatile Organic Compounds) emissions are separated depending on sources. Global anthropogenic emissions are given by the GEIA (Wang et al., 1998) and EGDAR (Olivier, 2005) inventories and regional anthropogenic emissions are specially estimate for US (NEI05), Canada (CAC), Mexico (BRAVO), Europe (EMEP) and East Asia (Streets et al., 2006; Zhang et al., 2009). Fossil fuel emissions are provided by EPA and STREETS 2006 inventories (Yevich and Logan, 2003), biomass burning emissions by GFED inventory (Lobert et al., 1999), and biogenic emissions by the MEGAN model calculations (Guenther et al., 2012). In addition, $NO_x$ from soil emissions are calculated by an algorithm depending on temperature and precipitation (Yienger and Levy, 1995).

The lightning $NO_x$ emissions calculation is initially based on the cloud-top-height parameterization (Price and Rind, 1992, 1994) with a “C-shaped” profile describing $LNO_x$ vertical distribution (Pickering et al., 1998; Ott et al., 2010). Lightning flashes are constrained using the climatologies from the LIS/OTD observations (Sauvage et al.,

2007b; Murray et al., 2012). Global lightning $NO_x$ emissions are also constrained to 6 Tg N $yr^{-1}$ in order to match to satellite observations (Martin et al., 2007).

### 2.2 The Meso-NH model

The Meso-NH model is an atmospheric model developed jointly by the Laboratoire d'Aérologie and by CNRM-GAME (http://mesonh.aero.obs-mip.fr/mesonh51). The model includes a non-hydrostatic and anelastic system of equations (Lafore et al., 1998) and has a complete set of parameterizations allowing to reproduce physical processes such as radiation (Gregory et al., 2000), atmospheric turbulence (Cuxart et al., 1999), convection (Bechtold et al., 2000), microphysics related to warm clouds (Cohard and Pinty, 2000), and atmospheric ice (Pinty and Jabouille, 1999; Lascaux et al., 2006). Meso-NH includes also on-line chemistry (Tulet et al., 2003, 2006). The model deals with large (synoptic) to small (large eddy) scales. In this study, the Mesonh-49 version was used in order to compare the horizontal diffusion coefficient ($D_h$) estimate within the anvil of thunderstorms from in-situ measurements to a modeling ideal case of a convective cell.

### 2.3 The DSMACC chemical box model

The Dynamical Simple Model of Atmospheric Chemical Complexity (DSMACC) is a simple box model developed for improving our understanding of the tropospheric chemistry (Emmerson and Evans, 2009). The model is composed of the KPP chemical pre-processor (Damian et al., 2002) to solve differential equations representing the chemical system. The TUV (Tropospheric Ultraviolet and Visible Radiation Model) photolysis scheme is used, which calculates the spectral irradiance, the spectral actinic flux, photodissociation coefficients (*J* values) (Madronich and Flocke, 1999), and biologically effective irradiance. The chemical scheme used derives from the Master Chemical Mechanism (MCM, http://mcm.leeds.ac.uk/MCM/), (Jenkin et al., 1997;



Saunders et al., 2003), which contains 17 000 elementary reactions of 6700 primary, secondary and radical species.

In order to study the chemical interactions that could occur in the undiluted plume fraction, a set of short simulations was carried out with the DSMACC chemical box model as explained in the Sect. 3.2.2.

## 3 Plume parameterization for lightning $NO_x$ emissions

### 3.1 General description

The $LNO_x$ plume parameterization is based on a method initially developed by Cariolle et al. (2009) for $NO_x$ emissions related to aircraft exhausts later adapted to ship emissions of $NO_x$ (Huszar et al., 2010). In this approach, the plume effects at sub-grid scale are represented via a fuel tracer, to follow the amount of the emitted species in the plume and an effective reaction rate for the ozone production and nitric acid production/destruction during the plume's dilution into the background (Cariolle et al., 2009; Paoli et al., 2011). The parameterization requires a proper estimation of the characteristic plume lifetime during which the non-linear interactions between species are important and simulated via specific rates of conversion. The approach ensures the mass conservation of species in the model. This is the only method which considers a plume evolution related to the local $NO_x$ emissions allowing the transport of the non-linear effects occurring at smaller scale than the model grid.

#### 3.1.1 Physical plume formulation

Following Cariolle et al. (2009), a passive tracer (from the perspective of the usual model chemistry) is added to the model to represent $NO_x$ emitted by lightning. Rather than increasing the concentration of the $NO_x$ tracer in the model, lightning $NO_x$ emissions now increase the concentration of this new tracer which is transported in the

standard way by advection and turbulence. Plume chemistry is considered to be significant when the concentration of the lightning $NO_x$ tracer is higher than a critical $NO_x$ content, hereafter denoted $r_l$. Above this value the lightning $NO_x$ tracer is transferred to the normal $NO_x$ tracer at a rate described by a plume lifetime ($\tau$), which is an exponential decay constant. This corresponds to an exchange time scale between the lightning $NO_x$ plume and the background $NO_x$. The continuity equation related to the tracer evolution is detailed by the Eq. (1).

$$\frac{\partial \overline{r_{LNO_x}}}{\partial t} + \langle F_{LNO_x} \rangle = I - \frac{1}{\tau} \times \overline{r_{LNO_x}} \quad (1)$$

where $\overline{r_{LNO_x}}$, is the concentration (in molecules cm$^{-3}$) of the $NO_x$ lightning tracer in the model grid (note that all overlined terms referred to grid average quantities in the CTM), $F_{LNO_x} \equiv \nabla \times (\overline{r_{LNO_x}} u) + \nabla \times (D_t \nabla \overline{r_{LNO_x}})$ and it corresponds to the flux divergence related to the large-scale transport of the tracer (advection and turbulent diffusion, in molecules cm$^{-3}$ s$^{-1}$), $I$ is the injection rate of $NO_x$ (in molecules cm$^{-3}$ s$^{-1}$) and $\tau$ is the plume lifetime (in seconds).

The calculation of $\tau$ requires evaluating the mass fraction of the lightning $NO_x$ ($M(t)$) corresponding to the undiluted fraction of the plume and characterized by a $NO_x$ concentration above the $r_l$ critical value. In other words, the plume boundary is defined by the critical value $r_l$ depending on the time of day. The $NO_x$ mass, $M(t)$ decreases monotonically to zero until $t = T_l$ for which the tracer concentration is everywhere below the $r_l$ threshold. The plume lifetime is obtained by an exponential function depending on the mass (Eqs. 2 and 3):

$$M(t) = \int_{V_p} \rho \times r_p \times dV \quad (2)$$

$$\tau = \int_{t_0=0}^{+\infty} \exp(-t/\tau) \times dt = \frac{1}{M(t_0)} \int_{t_0=0}^{T_l} M(t) \times dt \quad (3)$$



where $V_p$ is the volume of the plume, $\rho$ is the density of the air, $r_p$ is the $NO_x$ concentration within the plume (molecules cm$^{-3}$) and $T_l$ is the time for which the concentration $r_p$ is everywhere below the critical value $r_l$. The calculation of the plume lifetime, by simple plume dispersion simulations, depends on (i) the initial emissions of $NO_x$ by lightning, (ii) the $r_l$ value, and (iii) the dispersion properties of the atmosphere (related to the horizontal diffusion coefficient, $D_h$) and is detailed on the Sect. 3.2.3. Note that the mean dispersion properties of the atmosphere were associated with the horizontal diffusion only. The vertical diffusion is less efficient than the horizontal one (Cariolle et al., 2009) and it is not considered in this study. In addition, the vertical dispersion of the plume is related to the vertical distribution of $LNO_x$ a priori forced in the GEOS-Chem model by the C-shape profile (Ott et al., 2010) and it is beyond the scope of this study.

### 3.1.2 Plume chemistry of $NO_x$, $O_3$ and $HNO_3$

Once the lightning $NO_x$ is emitted, it is transferred to model's background $NO_x$ based on the lifetime of the plume ($\tau$). Thus, the continuity equation for the $NO_x$ species emitted in the plume and released to the large scale can be deduced as described by the Eq. (4).

$$\frac{\partial \overline{r_{NO_x}}}{\partial t} + \langle F_{NO_x} \rangle = +\frac{1}{\tau} \times \overline{r_{LNO_x}} \times \alpha_{NO_x} \times EI_{NO_x} + L_{ss} \quad (4)$$

where $\overline{r_{NO_x}}$, is the concentration of $NO_x$ (molecules cm$^{-3}$) in the model grid, $\alpha_{NO_x}$ is the molecular mass ratio between the air and $NO_x$ species, $EI_{NO_x}$ is the emission index for $NO_x$ (in g kg$^{-1}$) and $L_{ss}$ are the large-scale sources and sinks (in molecules cm$^{-3}$ s$^{-1}$) such as natural and anthropogenic emissions, photochemical reactions, mixing, and conversion to reservoir species.

We consider a fairly simple chemistry within the plume as described below. The increase of the nitrogen oxides concentration in the upper troposphere leads to ozone production through the reaction of NO with peroxyde ($HO_2$), $CH_3O_2$, or $RO_2$ radicals

from the OH oxydation as shown by the Reaction (R1).

$$NO + RO_2 \longrightarrow NO_2 + RO \quad (R1)$$

In the case of large $NO_x$ injection by lightning, the $NO_x$ content ($\sim 40$ ppt in unpolluted atmosphere) becomes of the same order (a few ppb, according to in-situ measurements, Dye et al., 2000; Huntrieser et al., 2002) than the surrounding ozone ($60 \pm 24$ ppb) (Jaéglé et al., 1998). The ozone evolution within the plume is described by the Reactions (R2)–(R6).

$$NO_2 + h\nu(\lambda < 400\,\text{nm}) \longrightarrow NO + O \quad (R2)$$
$$NO + O_3 \longrightarrow NO_2 + O_2 \quad (R3)$$
$$O + O_2 + M \longrightarrow O_3 + M \quad (R4)$$
$$O + NO_2 \longrightarrow NO + O_2 \quad (R5)$$
$$O + O_3 \longrightarrow 2O_2 \quad (R6)$$

From these equations we can define an $O_x$ family ($O_x \equiv O + O_2 + NO_2$) where the only net loss of $O_x$ is by reactions between atomic oxygen and $NO_2$ or $O_3$. The sums of the concentrations as detailed by the Eqs. (5)–(7) (Cariolle et al., 2009).

$$\frac{d(O + O_3)}{dt} = +k_2 \times NO_2 - k_3 \times NO \times O_3 - k_5 \times O \times NO_2 - 2 \times k_6 \times O_3 \times O \quad (5)$$
$$\frac{d(O + O_3 + NO_2)}{dt} = -2 \times k_5 \times O \times NO_2 - 2 \times k_6 \times O_3 \times O \quad (6)$$
$$\frac{d(NO + NO_2)}{dt} = 0 \quad (7)$$

where $k_i$ correspond to the rate constants for the $R_i$ reactions.

Thus two processes occur to $O_3$ in the plume at daytime. On short timescales $O_x$ is conserved. Lightning emissions of NO in the plume are converted into $NO_2$ but as $NO_2$ is in $O_x$ family, there is net conservation of $O_x$. However, on long timescales $O_x$ can be



destroyed through the reaction of O with $NO_2$ and $O_3$. Both of these processes need to be considered.

The first regime (regime I) occurs at low concentrations of $NO_x$ (relative to $O_3$). Under these conditions the Reaction (R5) is slow. There is the rapid equilibrium between NO, $NO_2$ and $O_3$ (Reactions R2–R4). As a consequence, $O_3$ is converted into $NO_2$ and can be restored later after dilution of the plume depending on the balance between NO and $NO_2$ at the large scale (Cariolle et al., 2009). Overall $O_x$ is conserved. In this regime NO emitted reacts with the available $O_3$ until the NO to $NO_2$ ratio in the plume reaches that in the background. Thus the impact on the $O_3$ background concentration is to reduce it by the number of molecules of NO emitted multiplied by the background $NO_2$ to $NO_x$ ratio. The effect of the first regime on the ozone burden is expressed by the Eq. (8).

$$\frac{\partial \overline{r_{O_3}}}{\partial t} + \langle F_{O_3} \rangle = -\frac{1}{\tau} \times \overline{r_{LNO_x}} \times \alpha_{NO_x} \times EI_{NO_x} \times \left( \frac{\overline{NO_2}}{\overline{NO_x}} - E \right) \times \delta + L_{ss} \quad (8)$$

where $\overline{r_{O_3}}$ is the concentration of $O_3$ (molecules cm$^{-3}$) in the model grid, $E$ is the $\frac{NO_2}{NO_x}$ ratio in the initial emissions, $\delta$ is equal to 1 during the day and 0 at nighttime, $L_{ss}$ are the sources and sinks of ozone such as photochemical production, transport from the stratosphere, surface deposition, photolysis reactions, and photochemical destruction.

The second regime (regime II) occurs at high concentrations of $NO_x$ (relative to $O_3$). Under these conditions the rate of Reaction (R5) is large. The non-linear chemical interactions between $NO_x$ and $O_3$ occur with different rates than in the background atmosphere. To account for this, Cariolle et al. (2009) introduced an effective reaction rate constant ($K_{eff}$), which is related to the production or the destruction of the odd oxygen ($O_x$) within the plume. $K_{eff}$ is expressed by the Eq. (9).

$$K_{eff} = \frac{\int_{t_0}^{T_l} \int_{V_p} K \times r^P_{NO_x} \times r^P_{O_3} \times dV_p \times dt}{\overline{r_{O_3}} \times \int_{t_0}^{t_l} \int_{V_p} r^P_{NO_x} \times dV_p \times dt} \quad (9)$$

where $r^{P}_{NO_x}$ and $r^{P}_{O_3}$ are the concentrations of nitrogen oxides and ozone within the plume and $K$ is the rate of $NO_x$-$O_3$ reaction within the plume.

The analysis of the chemical reactions related to the two regimes shows that $O_3 \gg O$ and $k_5 \times NO_2$ is more efficient than $k_6 \times O_3$ as a sink for $O_x$ (Cariolle et al., 2009). Thus, the Eq. (6) is simplified to give the Eq. (10).

$$\frac{d(O_3 + NO_2)}{dt} = -2 \times k_5 \times O \times NO_2 \tag{10}$$

Consequently, $K_{eff}$ can be simplified to Eq. (11).

$$K_{eff} = \frac{2 \times \left( \int^{T} k_5 \times O \times NO_2 \times dt \right)}{\left( NO_x \times \int^{T} O_x \times dt \right)} \tag{11}$$

The calculation of $K_{eff}$ is detailed in Sect. 3.2.4. Considering the two regimes related to the sub-grid plume chemistry, the ozone burden is described by the Eq. (12) at daytime and nighttime. Note that at nighttime there is no direct impact due to the ozone plume chemistry on its burden as $\delta = 0$. Only indirect effects are expected from $NO_y$ chemistry.

$$\frac{\partial \overline{r_{O_3}}}{\partial t} + \langle F_{O_3} \rangle = -\frac{1}{\tau} \times \overline{r_{LNO_x}} \times \alpha_{NO_x} \times EI_{NO_x} \times \left( \frac{\overline{NO_2}}{\overline{NO_x}} - E \right) \times \delta - K_{eff} \times \overline{r_{LNO_x}} \times \rho \times \alpha_{NO_x} \times EI_{NO_x} \times \overline{r_{O_3}} \times \delta + L_{ss} \tag{12}$$

In addition, we consider the conversion of $NO_x$ into $HNO_3$ within the plume. This conversion takes place in two different ways depending on the day or night atmospheric conditions. During the day, $NO_2$ reacts with OH to give $HNO_3$ directly and it is characterized by the coefficient $\beta_1$. While at nighttime the conversion of $NO_x$ to $HNO_3$ occurs



through $N_2O_5$ formation followed by a heterogeneous hydrolysis reaction, which corresponds to $\beta_2$. These two fractions are unitless.

In summary, the equation system solved at large scale by the CTM for lightning $NO_x$ source is detailed by the Eqs. (13)–(15).

$$\frac{\partial \overline{r_{NO_x}}}{\partial t} + \langle F_{NO_x} \rangle = +\frac{1}{\tau} \times \overline{r_{LNO_x}} \times (1 - \beta_1 \times \delta - \beta_2 \times (1 - \delta)) \times \alpha_{NO_x} \times EI_{NO_x} + L_{ss} \tag{13}$$

$$\frac{\partial \overline{r_{HNO_3}}}{\partial t} + \langle F_{HNO_3} \rangle = +\frac{1}{\tau} \times \overline{r_{LNO_x}} \times (\beta_1 \times \delta + \beta_2 \times (1 - \delta)) \times \alpha_{NO_x} \times EI_{NO_x} + L_{ss} \tag{14}$$

$$\frac{\partial \overline{r_{O_3}}}{\partial t} + \langle F_{O_3} \rangle = -\left( \frac{1}{\tau} \times \left( \frac{\overline{NO_2}}{\overline{NO_x}} - E \right) + K_{eff} \times \overline{r_{O_3}} \times \rho \right) \times \overline{r_{LNO_x}} \times \alpha_{NO_x} \times EI_{NO_x} \times \delta + L_{ss} \tag{15}$$

where $\overline{r_{NO_x}}$, $\overline{r_{HNO_3}}$ and $\overline{r_{O_3}}$ correspond to the $NO_x$, $HNO_3$ and $O_3$ concentrations averaged over the grid cell of the model, respectively.

In this study, the tropospheric chemistry and especially the $LNO_x$ plume chemistry is considered both at daytime and nighttime since all reactions are not initiated during the day. The chemical interactions during the night correspond mainly to the reactions of $O_3$ and O with NO and $NO_2$ as well as the $NO_x$ deactivation and the chemistry of the nitrogen reservoir species ($HNO_3$, $N_2O_5$ and PAN) and the nitrate radical ($NO_3$). $NO_3$ is the main oxidant in night conditions and it is produced from the slow oxidation of $NO_2$ by $O_3$ (Reaction R7).

$$NO_2 + O_3 \longrightarrow NO_3 + O_2 \tag{R7}$$

The other dominant source of $NO_3$ is the destruction of $N_2O_5$ (Reaction R8), but as $N_2O_5$ is formed from $NO_3$ (Reaction R9), the two species act in a coupled manner.

$$N_2O_5 + M \longrightarrow NO_3 + NO_2 + M \tag{R8}$$

$$NO_3 + NO_2 + M \longrightarrow N_2O_5 + M \quad \text{(R9)}$$

As mentioned previously, $N_2O_5$ is a determinant species for the tropospheric chemistry at nighttime allowing the $HNO_3$ formation by the heterogeneous reaction on the particle surface (aerosols and ice crystals). During the day, $NO_3$ rapidly undergo photolysis to produce NO or $NO_2$. In addition, $NO_3$ reacts very quickly with NO which is more concentrated at daytime than at nighttime (Reaction R10) but $NO_3$ is very low at daytime. However, this reaction can take place during the night especially for a plume characterized by high NO concentrations (lightning emissions) which is transported both during the day and night.

$$NO_3 + NO \longrightarrow NO_2 + NO_2 \quad \text{(R10)}$$

Furthermore, the nitrate radical can potentially reacts with VOCs. The reaction of the unsaturated hydrocarbons such as, isoprene, butenes, and monoterpenes, with $NO_3$ leads to the $HNO_3$ formation (Monks, 2005) (Reaction R11).

$$NO_3 + RH \longrightarrow HNO_3 + R \quad \text{(R11)}$$

Considering $NO_3$ reaction with alkenes, an additional mechanism is found initiating a complex chemistry allowing to form $NO_2$ or organic nitrates (Monks, 2005). Finally, $NO_3$ can initiate the VOCs oxidation via peroxy radical production (Reaction R12). That way, it can involve as a chain propagator (Reactions R13–R17).

$$NO_3 + \text{Organic Compound} \longrightarrow R + \text{Products} \quad \text{(R12)}$$
$$R + O_2 + M \longrightarrow RO_2 + M \quad \text{(R13)}$$
$$RO_2 + NO_3 \longrightarrow RO + NO_2 + O_2 \quad \text{(R14)}$$
$$RO + O_2 \longrightarrow R'R''CO + HO_2 \quad \text{(R15)}$$
$$HO_2 + O_3 \longrightarrow OH + 2O_2 \quad \text{(R16)}$$
$$HO_2 + NO_3 \longrightarrow OH + NO + O_2 \quad \text{(R17)}$$



The reactions of $HO_2$ with ozone (Reaction R16) or $NO_3$ (Reaction R17) imply OH production. Also, the reaction of ozone with alkenes allows to form OH during the night (Reaction R18) (Aumont, 2005).

$$\text{Alkene} + O_3 \longrightarrow v_1 OH + v_2 HO_2 + v_3 RO_2 \quad \text{(R18)}$$

The Reaction (R18) occurs when ozone concentrations remain sufficiently high in night conditions, in other words for polluted atmosphere.

In this context, we consider different values at daytime and nighttime for the plume lifetime, the effective reaction rate constant and for the fraction of $NO_x$ conversion into $HNO_3$ within the plume. Distinguishing day and night chemistry is linked with the fluctuation of the critical $r_l$ value (below which the sub-grid plume chemistry is negligible) depending on atmospheric conditions. Therefore, if $r_l$ changes with sunlight, the plume lifetime changes also. Note that except the $\beta_2$ fraction, this night chemistry is not considered by the initial plume approach developed by Cariolle et al. (2009), which considers $NO_x$ plumes from aircraft exhausts only at daytime.

Figure 1 summarizes all elements which define the plume approach and how it has been adapted and implemented into the model.

### 3.2 Parameter calculations for lightning $NO_x$ emissions

In order to reproduce more accurately the lightning $NO_x$ sub-grid chemistry, some points should be considered: (i) the latitude ($NO_x$ emissions by lightning are higher in tropics than in midlatitudes), (ii) the sunlight conditions (day and night) which impacts photochemistry and heterogeneous chemistry, (iii) the plume evolution with its own physical characteristics (the lifetime and the dispersion properties); and finally (iv) chemical interactions within the plume related to high concentrated fraction of $NO_x$ considerably higher than background concentrations. In the following section, physical and chemical characteristics of the plume associated with lightning $NO_x$ source have been defined.

### 3.2.1 Dynamical conditions

The horizontal diffusion coefficient ($D_h$) is a key parameter of the atmospheric dynamical conditions in determining the dispersion of the lightning $NO_x$ plume. $D_h$ is used as the dispersion constraint for the simple plume dispersion simulations carried out in order to estimate the plume lifetime and the effective reaction rate constant. The diffusion coefficient was defined by running the 3-D mesoscale Meso-NH model but mainly from previous in-situ measurement in thunderstorm anvil.

The Meso-NH mesoscale model was used (see Sect. 2.2) to investigate $D_h$. A simple convective cell forced by warm bubble and initialized by a radiosounding at the beginning of the simulation was run as an ideal case. Simulations were realized for a domain of 24 km in the two horizontal directions and the grid horizontal resolution is $\Delta x = \Delta y = 1$ km and $\Delta z = 500$ m. The convective cell is located at 43.29° N latitude and 0° longitude (Klemp and Wilhelmson, 1978). Simulations of 6 h were made allowing the complete development and the dissipation of the convective cell. $D_h$ has been calculated within the anvil using the mixing length diagnostic variable, hereafter denoted $L$, as described by the Eq. (16) (Cuxart et al., 1999).

$$D_h = \frac{2}{3} \times \frac{L}{4} \times e^{\frac{1}{2}} \tag{16}$$

At the mature stage of the cell, $D_h$ was calculated as $100\,m^2\,s^{-1}$ within the upper levels of the convective cell (i.e. in the anvil, defined empirically).

In addition to modeling estimate, we used in-situ measurements to calculate $D_h$. Turbulence measurements were performed by a B-757 commercial aircraft along a fight from the west of Kansas to the north of Missouri and corresponding to a trajectory of more than 500 km (Trier and Sharman, 2008). These in-situ measurements were accomplished from 07:00 to 10:00 UTC the 17 June 2005, during the development of a mesoscale convective system (MCS). This MCS is associated with a turbulence event characterized by the measurement of the atmospheric eddy dissipation rate ($\epsilon$) and the turbulence kinetic energy (TKE) above and within the cloud anvil. The higher values of $\epsilon$



($\epsilon^{1/3} \sim 0,4\,m^{2/3}\,s^{-1}$) were recorded between 11.3 and 11.6 km altitude corresponding to the cloud anvil levels. In addition, for this MCS, the TKE was about $1\,m^2\,s^{-2}$ at the locations of the highest $\epsilon$ values.

According to these observations, the turbulent diffusivity (Eq. 17) was estimated above the anvil of the MCS (http://www.ral.ucar.edu/projects/turb_char/) such as: $D_h > 0.1\,m^2\,s^{-2}$. Then, $D_h$ was calculated within the anvil such as: $D_h = 15\,m^2\,s^{-1}$ using the same formulation (Eq. 17). This last estimate seems to be the most common value compared to the diffusion coefficient value of $20\,m^2\,s^{-1}$ used by Cariolle et al. (2009), close to the tropopause level and the $D_h$ value calculated for contrails ($15\,m^2\,s^{-1}$) in the upper troposphere (Knollenberg, 1972).

$$D_h = \frac{(\mathrm{TKE})^2}{\epsilon} \tag{17}$$

The $D_h$ estimate using Meso-NH model is high compared to the results from measurements and corresponds to the upper limit of the calculated diffusion coefficients and could be associated with the turbulence in the convective cloud. However, it is important to note that usually most numerical simulations are performed with 1-D turbulence models. What is interesting in the use of Meso-NH in this study is that the 3-D turbulence is solved. This simulation provides an additional estimate of $D_h$ allowing comparison with the calculation from in-situ measurements. Moreover, studies on the diffusivity in cloud anvils are uncommon. It is necessary to conduct additional work in the future on that issue again constrained with new in-situ measurements of the atmospheric turbulence in the anvil.

In order to cover all of horizontal diffusivity estimates discussed in this section the range of values 0.1, 15 and $100\,m^2\,s^{-1}$ was used. Hereafter, the results are detailed for the central value $D_h = 15\,m^2\,s^{-1}$. Sensitivity tests depending on the uncertainty associated with the parameter estimate are performed and presented later in Sect. 4.3.

### 3.2.2 The $NO_x$ critical plume content ($r_l$)

The $r_l$ critical value is the $NO_x$ concentration within the undiluted phase of the plume below which the non-linear chemistry can be neglected (Sect. 3.1). It has been estimated using the 0-D DSMACC chemical box model (Sect. 2.2). Initial conditions for simulations carried out with the DSMACC box model are from outputs of the GEOS-Chem model. Especially, initial atmospheric parameters and atmospheric background concentrations of species correspond to the average of the GEOS-Chem outputs (i) from 8 to 11 km, (ii) for two latitude regions (tropics and midlatitudes), and (iii) for the year 2006 (Table 1).

In order to focus on chemistry interactions only between chemical species of interest and removing the mixing influence and sunlight fluctuations, short simulations (i.e. one hour each) were run with the DSMACC model. The effects of the day or night conditions were carefully considered carrying out separate simulations at daytime and nighttime. Simulations were run for a large range of initial NO concentrations from 0.01 ppb to 1 ppm. The $r_l$ value is defined from the NO value for which the $\frac{\partial O_x}{dt}$ trend is perturbed. In other words, $r_l$ is associated to the second derivative of $O_x$, i.e. the curve optimums on Fig. 2. The $r_l$ threshold was defined as to be 0.1 and 0.25 ppb during the day and night for midlatitudes and 0.1 and 0.75 ppb during the day and night in tropics (Fig. 2).

Note that the midlatitudes and the tropics were separated because of the large differences in $LNO_x$ emissions between the two regions in terms of the number of flashes in a particular convective cell which is higher in the tropics according to the LIS/OTD climatologies (Christian et al., 2003). This last point is important for the plume lifetime estimate detailed in the following section.

### 3.2.3 The plume lifetime $\tau$

The plume lifetime ($\tau$) depends directly on (i) the initial NO pulse from lightning emissions, (ii) the $r_l$ critical value, and (iii) the diffusion properties of the atmosphere. The plume lifetime also depends on the initial size of the plume. Here we use a width of



500 m to refer to an ensemble of spikes at the cloud scale. $\tau$ is crucial for the physical description of the $NO_x$ plumes and it has been computed in carrying out dispersion simulations of a simple plume assumed to be cylindrical. The simple model is composed of 30 levels of dispersion. In the model, the standard atmospheric conditions are represented by temperature, pressure and species concentrations of the background atmosphere which are similar to the initial conditions used for the DSMACC simulations. As a reminder, initial conditions are from GEOS-Chem outputs averaged (i) from 8 to 11 km, (ii) for two latitude regions (tropics and midlatitudes), and (iii) for the year 2006 (Table 1). Simulations are initialized by a NO pulse from lightning emissions (hereafter denoted $NO_i$) and the plume dispersion depends on the $D_h$ value estimated in Sect. 3.2.1.

The initial tracer concentrations $NO_i$ related to lightning NO emissions at the scale of a convective cell (gathering several flashes together) in midlatitudes were defined according to previous aircraft measurement campaigns. Especially, the STERAO campaign recorded NO spikes of magnitude from 1–10 ppb related to lightning activity in thunderstorms occurring 9–10 July 1996 over the northern Colorado (Dye et al., 2000; Stith et al., 1999). Lange et al. (2001) measured NO spikes of 3.5 ppb during the STREAM campaign associated with a matured storm over the Ontario. Several peaks of NO mixing ratios from 0.7–6 ppb were also observed during EULINOX (Huntrieser et al., 2002) over Germany in July 1998. The LINOX aircraft campaign recorded NO spikes from 0.75–1.25 ppb (Huntrieser et al., 1998) related to thunderstorm over Europe, the 30 July 1996. From these studies, the NO concentration associated with the electrical activity in thunderstorms occurring over midlatitudes was determined as $NO_i^{\text{mean, Midlats}} = 3.4$ ppb ($NO_i^{\text{min, Midlats}} = 0.7$ and $NO_i^{\text{max, Midlats}} = 10$ ppb). Because there are much fewer $LNO_x$ measurements in the tropics and in order to be consistent with the $LNO_x$ emissions defined in the GEOS-Chem model, the ratio $R_{LNO_x} = \frac{LNO_x^{\text{Midlatitudes}}}{LNO_x^{\text{Tropics}}}$ was defined as in the CTM. During the year 2006, the relative midlatitudes and tropics $LNO_x$ contribution was about $R_{LNO_x} = 0.33$. This result

is in agreement with higher $LNO_x$ emissions in these regions rather than in midlatitudes. The value of NO mixing ratio injected by lightning in tropics was defined as $NO_i^{mean,\ Tropics} = 10.2$ ppb ($NO_i^{min,\ Tropics} = 2.8$ and $NO_i^{max,\ Tropics} = 29.7$ ppb).

Once $NO_i$ estimate was completed, the calculation of the plume lifetime was achieved using the detailed formulation given in Sect. 3.1.1. The results for $\tau$ are summarized in Table 2. Hereafter, the results are detailed for $NO_i^{mean}$ in Sect. 4 and sensitivity tests are carried out using all $NO_i$ values for midlatitudes and tropics (Sect. 5). Model calculations for $NO_i^{mean}$ and $D_h = 15\,m^2\,s^{-1}$ provide a minimum plume lifetime of 3 (6) h for midlatitudes and maximum plume lifetime of 9 (21.3) h for tropics at daytime (nighttime).

### 3.2.4 The effective reaction rate constant ($K_{eff}$)

The non-linear chemistry within the plume has been considered in calculating the effective reaction rate constant ($K_{eff}$), which is used to compute the formation of the secondary species ($O_x$ and $HNO_3$) within the plume. That corresponds to the evolution of odd oxygen depending on the O and $O_3$ reactions with $NO_2$ and NO, and also on the $NO_x$ activation (day) or deactivation (night) with the $HNO_3$, $N_2O_5$ and PAN chemistry.

$K_{eff}$ is calculated according to the Eq. (11) of the Sect. 3.1.2 using the same simple plume dispersion simulations than those carried out to define the plume lifetime (Sect. 3.2.3).

Results for $K_{eff}$ are summarized in Table 3. Model calculations using $NO_i^{mean}$ and $D_h = 15\,m^2\,s^{-1}$ give a $K_{eff}$ value of $5.49 \times 10^{-19}$ molecules$^{-1}$ s$^{-1}$ cm$^{-3}$ ($4.55 \times 10^{-19}$ molecules$^{-1}$ s$^{-1}$ cm$^{-3}$) in midlatitudes and $3.64 \times 10^{-19}$ molecules$^{-1}$ s$^{-1}$ cm$^{-3}$ ($2.98 \times 10^{-19}$ molecules$^{-1}$ s$^{-1}$ cm$^{-3}$) in tropics, at daytime (at nighttime).

$K_{eff}$ estimations obtained in this study are very low as well as those calculated by Cariolle et al. (2009), for the plume chemistry related to aircraft exhausts. In this previous work, $K_{eff}$ varies from 1.0 to $4.2 \times 10^{-18}$ molecules$^{-1}$ s$^{-1}$ cm$^{-3}$ with a mean value close to $3 \times 10^{-18}$ molecules$^{-1}$ s$^{-1}$ cm$^{-3}$ depending on the $NO_x$ loading. The very low



value for $K_{eff}$ point out that the plume parameterization implies a delay of the production of ozone at the large scale rather than its destruction within the plume.

### 3.2.5 The fractions of $NO_x$ conversion to $HNO_3$ ($\beta_1$ and $\beta_2$)

The fractions $\beta_1$ and $\beta_2$ represent the $NO_x$ conversion into $HNO_3$ within the plume at daytime and nighttime respectively. They were computed using the DSMACC chemical box model.

The $\beta_1$ coefficient was calculated for day conditions depending mainly on the OH concentration. The conversion of $NO_x$ into $HNO_3$ at nighttime ($\beta_2$ coefficient) is related to the heterogeneous reaction of $N_2O_5$ and so depends on particles (aerosols and ice crystals) concentration and their lifetime. This is directly linked with the surface density and the radius of particles in the anvil region of thunderstorms, which is highly uncertain. We defined these values using in situ measurements. The surface area ($S_T$) and the radius ($R$) for aerosols are defined such as: $S_T = 0.28\,m^{-1}$ and $R = 1\,\mu m^{-1}$ (Huntrieser et al., 2002) and for ice, $S_T = 0.03\,m^{-1}$ and $R = 30\,\mu m^{-1}$ (Knollenberg et al., 1993). In addition, the reaction probabilities of $NO_x$ on aerosols and ice crystals $\gamma_{N_2O_5}^{aerosols} = 0.02$ (Evans and Jacob, 2005) and $\gamma_{N_2O_5}^{ice} = 0.03$ (Sander et al., 2006), respectively, were used for our box model simulations. These values correspond to the probability that a $N_2O_5$ molecule impacting an aerosol or an ice crystal surface was subjected to react. The results for $\beta_1$ and $\beta_2$ coefficients are summarized in Table 4.

The estimate of $\beta_1$ fraction does not show significant variation neither between latitudes regions nor depending on $NO_i$. The minimum $\beta_1$ value is $1.34 \times 10^{-4}$ for tropical regions and $NO_i^{min}$, and the maximum $\beta_1$ value is $1.88 \times 10^{-4}$ for midlatitudes and $NO_i^{max}$. The study of production and destruction rates for day conditions taking into account all reactions pathways (not shown here) demonstrates that production of $HNO_3$ during the day is mainly determined by reaction of $NO_3$ with formaldehyde (HCHO) and acetaldehyde ($CH_3CHO$). Surprisingly, $HNO_3$ formation via the $NO_2 + OH$ reaction

seems to be less efficient. This result could be explained by the low initial concentrations of OH used for the DSMACC simulations and it is in agreement with the small $\beta_1$ values. Then, the averaged $\beta_2$ coefficient is higher by a factor 10 compared to $\beta_1$ with a minimum value of $0.24 \times 10^{-3}$ in tropics for $NO_i^{max}$ and a maximum estimate of $14.4 \times 10^{-3}$ in midlatitudes for $NO_i^{min}$. The analysis of the production and the destruction rates for night conditions taking into account all reactions pathway shows that the predominant reaction in the $HNO_3$ evolution is $N_2O_5 + H_2O$ (or the heterogeneous reaction on the aerosols and ice crystals surface).

## 4 Results: CTM simulations

In this section, the effects of the lightning $NO_x$ plume parameterization, i.e. the influence of sub-grid processes related to lightning emissions, on the $NO_x$ and $O_3$ tropospheric distributions at large scale are evaluated. Then, the parameterization sensitivity to initial NO mixing ratio injected by lightning ($NO_i$), $D_h$, $\beta_1$ and $\beta_2$ coefficients is analyzed to quantify the variability of the results regarding the plume-in-grid parameter calculations.

### 4.1 Implementation of the $LNO_x$ plume parameterization

The implementation of the lightning $NO_x$ plume parameterization into the GEOS-Chem model requires specifying the system of continuity equations related to the plume chemistry solved at large scale by the model (Sect. 3.1.2, Eqs. 13–15). Lightning $NO_x$ emissions calculated in each grid box (in molecules $cm^{-2}\,s^{-1}$) by the model are directly used to compute the injection rate $I$ ($s^{-1}$) of NO at each chemical time step of the simulation. Then, we consider the following setup: $\alpha_{NO_x} = 1$ and $EI_{NO_x} = 1$, in order to represent the mixing ratio of the undiluted fraction of $NO_x$ by the tracer ($r_{LNO_x}$). Furthermore, lightning produce only NO among $NO_x$ species thus $E = 0$ in the Eq. (15).



Finally, the ratio $\frac{\overline{NO_2}}{\overline{NO_x}}$ is the relative balance between NO and $NO_2$ in the diluted phase at large scale reproduced by the model.

### 4.2 Impact of $LNO_x$ emissions on the $NO_x$ and $O_3$ distributions

We perform a spin-up of six months (from July 2005 to January 2006) in order to obtain a steady state in the model after activation of the plume parameterization. Then simulations were run for the entire year 2006. The transport and the convection time steps are 15 min and the emissions and the chemical time steps are 30 min.

In the following, standard simulation refers to simulation with standard lightning $NO_x$ emissions i.e. instantaneously diluted in a grid cell, while modified simulation refers to simulation considering the plume parameterization and then sub-grid chemistry. Note that the modified simulation was run using mean values for the initial NO mixing ratio ($NO_i^{mean,\,Midlats} = 3.4$ ppb and $NO_i^{mean,\,Tropics} = 10.2$ ppb) and $D_h = 15\,m^2\,s^{-1}$. The Base Case (BC) experiment corresponds to the standard simulation minus the standard simulation without lightning $NO_x$ emissions. The P1 experiment corresponds to the modified simulation minus the standard simulation without lightning $NO_x$ emissions. The P2 experiment is the same as the P1 experiment but without considering the nitrification mechanism in the modified simulation (i.e. $\beta_1 = \beta_2 = 0$). In addition, sensitivity tests were performed for P1 defined by the modified simulation using the minimum and the maximum values for $D_h$, $NO_i$, $\beta_1$ and $\beta_2$ coefficients. All experiments are summarized in Table 5.

Lightning emissions rates and the associated $LNO_x$ tracer distributions are first discussed, then the effects of the implementation of the plume parameterization (P1) compared to the experiment without the plume-in-grid development (BC case) is presented.

#### 4.2.1 Lightning emissions and $LNO_x$ tracer distributions

Figure 3 displays the geographical distributions of the 9 km lightning $NO_x$ emissions (a), the related $LNO_x$ tracer distributions (b) and the $LNO_x$ tracer zonal averaged (c) in January (top panels) and in July (bottom panels) reproduced by the CTM from the P1 experiment. These results are shown for an approximate detrainment level (9 km altitude) where the $LNO_x$ are the most concentrated. In January, the highest emissions of $NO_x$ from lightning ($4-6\times10^9$ molecules cm$^{-2}$ s$^{-1}$) are located in the Southern Hemisphere around the tropics over West Australia and Central-South Africa. Also, the model gives low $LNO_x$ emissions ($<3\times10^9$ molecules cm$^{-2}$ s$^{-1}$) over South America and North America especially over the Gulf of Mexico. In July, the highest $LNO_x$ emissions ($4-6\times10^9$ molecules cm$^{-2}$ s$^{-1}$) are calculated in the Northern Hemisphere over North America, North of India, Central Africa and Sahel. In addition, $LNO_x$ emissions are modeled over Europe and over East Asia but to a lesser extent ($<2\times10^9$ molecules cm$^{-2}$ s$^{-1}$).

The lightning $NO_x$ tracer introduced into the model represents the lightning $NO_x$ emissions affected by the transport and the exponential decay depending on the plume lifetime. Figure 3 shows that the tracer distribution is consistent with the lightning $NO_x$ emissions. However, it is important to note that the plume lifetime is a key factor in the evolution of the $LNO_x$ tracer mixing ratio. A long plume lifetime (several hours to several days) allows the intercontinental transport of $LNO_x$ plumes. The representation of the sub-grid chemistry and the transport of the non-linear chemistry effects related to the plume consideration becomes important for the chemistry of the regions located far downwind from source regions. According to its preliminary calculation (Sect. 3.2.3), the plume lifetime is longer in tropics (9 and 21.3 h for day and night conditions, respectively) than in midlatitudes (3 and 6 h, for day and night conditions, respectively). So, the $LNO_x$ tracer is characterized by a shorter lifetime as a plume over North America than over Central Africa and around the Sahel while the model simulated less important emissions over these regions especially in summer. In boreal winter, the mixing



ratio of the lightning $NO_x$ tracer calculated by the model is about 0.21 ppb over Central and South Africa, 0.18 ppb over West Australia and 0.11 ppb over South America. In summer, the tracer mixing ratio is simulated as 0.21, 0.32 and 0.16 ppb over Central Africa, North India and North America, respectively. The lightning $NO_x$ tracer is mainly reproduced at altitudes where lightning $NO_x$ are produced and detrained (in the upper troposphere) as shown in panels (c) in Fig. 3.

#### 4.2.2 Impact of lightning on $NO_x$ and $O_3$ distributions with the plume parameterization

The difference between P1 and BC experiments (P1 – BC) was calculated in order to quantify the changes on $NO_x$ and $O_3$ mixing ratios at large scale implied by the implementation of the plume-in-grid parameterization into GEOS-Chem. Figures 4 and 5 display the geographical distributions of the $NO_x$, $HNO_3$, PAN and $O_3$ absolute changes (in ppb) in January and in July, respectively. The 9 km altitude level was chosen because of the most significant variations at this altitude compared to the rest of the troposphere.

In boreal winter, $LNO_x$ plume chemistry leads to a maximum decrease at large scale over regions of emissions of 120 ppt for $NO_x$ and a decrease of 68 ppt for $HNO_3$ and 16 ppt for PAN over Central and South Africa. These variations are associated with a maximum $O_3$ decrease of 2.8 ppb over regions of emissions. A similar $NO_x$, $HNO_3$, PAN and $O_3$ reduction is obtained in other areas of high $LNO_x$ emissions (i.e. over West Australia and South America). Downwind of $LNO_x$ emissions the opposite effect is observed for $NO_x$ and $HNO_3$ species with maximum increase of 40 ppt for $NO_x$ and 13.5 ppt for $HNO_3$ observed over South Atlantic and Indian Ocean. Generally, PAN still decreases over oceans but in a lesser extent compared to regions of $LNO_x$ emissions, with a maximum reduction of 9 ppt. $O_3$ response is a maximum increase of 1.13 ppb around area where the transport is effective and especially over the oceans. In summer, maximum decreases of 140 ppt for $NO_x$ and 60 ppt for $HNO_3$ and 24 ppt for PAN are calculated by the CTM leading to a maximum $O_3$ decrease of 2.4 ppb over Cen-

tral Africa (reduction also observed over North America and North India). Downwind of lightning emissions, increase of $NO_x$ and $HNO_3$ is observed with a maximum value of 30 and 38 ppt, respectively. PAN reservoir species also still decreases slightly downwind with 2 ppt changes. Finally, that leads to maximum $O_3$ increase of 0.7 ppb.

Note that the production of PAN is limited by the supply of $NO_x$ or non-methane volatil organic compounds (NMVOCs). Above continental lightning sources regions, NMVOCs are uplifted by deep convection but with lower $NO_x$ due to the activation of the plume parameterization. That implies a less efficient PAN production in these regions. Downwind of lightning sources regions (oceanic regions), $NO_x$ increases because of the $LNO_x$ transport in plume form but there is less NMVOCs available to produce PAN. Therefore, the production is limited leading to an overall lower PAN production in P1.

In order to provide a full overview of the effects of the plume parameterization, the relative difference between the P1 and BC experiments (i.e. (P1–BC) /BC) was calculated integrated throughout the troposphere. Figures 6 and 7 show zonal averaged of $NO_x$ (upper panels) and $O_3$ (bottom panels) relative changes (in %) integrated throughout the troposphere for regions of interest for January and July, respectively. During boreal winter, the highest $NO_x$ ($O_3$) decreases of 10 % (5 %) in West Australia, then 20 % (6 %) in Central Africa are calculated. These negative variations are mainly calculated between 400 hPa and the tropopause level for $NO_x$ and ozone. South America is characterized by a decrease of 20 % of the nitrogen oxides and 1 % of ozone. Over this region, variations are significant in the entire troposphere for both species. In contrast to the continent decrease, $NO_x$ increase is observed over the major part of South Atlantic and Indian Ocean with 14 and 20 % maximum, respectively. The $O_3$ response in an increase of 1 % near the tropopause and it becomes higher close to the surface of about 4 %. In summer, there is a $NO_x$ ($O_3$) decrease of 25 % (8 %) over Central Africa, 20 % (2 %) over North India, and 5 % (0.5 %) over North America. Also, South Atlantic and Indian Ocean (located downwind of lightning $NO_x$ emissions) are characterized by a maximum increase of 18 % for $NO_x$ and 2 % for $O_3$.



As a result, the sub-grid chemistry associated to the $LNO_x$ emissions implies (i) a decrease of the nitrogen oxides and ozone mixing ratios at large scale over regions characterized by intense lightning emissions and (ii) an increase of these species downwind of emissions. Especially the plume parameterization related to the lightning $NO_x$ leads to:

1. Significant effects on $NO_x$ mixing ratio (±20 %): these effects on nitrogen oxides are important because $NO_x$ is the first criterion which is constrained in a CTM in order to determine the global $LNO_x$ production (6 Tg N $yr^{-1}$ in the GEOS-Chem model).
2. Lower effects on $O_3$ mixing ratio (±5 %): these limited impacts on ozone could be explained by compensatory effect of the $NO_y$ species (mainly conversion of $NO_x$ into (i) $HNO_3$ within the plume or (ii) PAN).

The effects of the plume parameterization are simulated over the entire troposphere mainly for ozone. Indeed, the spreading of effects on ozone to the lower free troposphere is related to the subsidence areas of the Walker circulation. These regions are characterized by accumulation and creation of ozone for low altitude levels. Nevertheless, the maximum $NO_x$ and $O_3$ variations are calculated for altitude levels associated with a mean detrainment level. The realistic representation of the sub-grid processes (P1 experiment) related to the $LNO_x$ plume is in contrast with the simplified instantaneous dilution in the grid cell of the lightning $NO_x$ emissions (BC experiment).

The plume approach allows the conversion of $NO_x$ into $HNO_3$ during the plume lifetime. In addition, the high $NO_x$ concentration within the plume (much higher than the background content) leads to the $O_3$ titration and more generally to the $O_x$ destruction within the plume. The most important impact of the plume parameterization is the transport of the $LNO_x$ emissions as a plume and the transport of the associated non-linear chemistry effects leading to a delay of the $O_3$ production at large scale. In other words, $O_3$ is less produced over the regions with intense lightning $NO_x$ emissions than downwind of $LNO_x$ emissions by photochemical reactions from $NO_x$.

### 4.3 Plume sensitivity to the estimated uncertainties of parameter calculations

#### 4.3.1 The Atmospheric dynamical conditions and the initial NO mixing ratio injected by lightning

The impact of (i) the diffusion properties of the atmosphere ($D_h$) and (ii) the initial NO mixing ratio injected by lightning ($NO_i$) are analyzed. $D_h$ and $NO_i$ are the two key parameters in the determination of the physical and chemical characteristics of the plume. The modified simulation characterizing the P1 experiment was run for the ranges of the horizontal diffusion coefficients and the initial NO mixing ratio injected by lightning. It is important to note that for these sensitivity tests, $\beta_1$ and $\beta_2$ coefficients remain constant using their mean values. $\tau$ and $K_{eff}$ values related to these simulations are those previously calculated (Sect. 3) and summarized in Tables 2 and 3. Figure 8 displays $\tau$ (upper panels) and $K_{eff}$ (bottom panels) variations depending on $D_h$ and $NO_i$. As expected, the strongest the horizontal diffusion is the most efficient the dispersion of the plume is. In both, midlatitudes and tropics, $\tau$ decreases when $D_h$ becomes larger. In addition, $\tau$ increases with the initial NO mixing ratio injected by lightning. In contrary, $K_{eff}$ increases with $D_h$ coefficient in the two regions of the globe.

The variability of $NO_x$ and $O_3$ mixing ratios around the mean value for regions and seasons depending on the known uncertainties associated with parameter calculations have been quantified. Figure 9 shows the intervals of variability of $NO_x$ and $O_3$ ($\Delta NO_x$ and $\Delta O_3$, respectively) at 9 km altitude reproduced by GEOS-Chem depending on $D_h$ and on the initial NO mixing ratio ($NO_i$). Note that for the sake of readability, the scale of $NO_x$ and $O_3$ changes differs by region. Results are also summarized in Table 6.

We chose representative continental areas such as Florida and Congo, which correspond to regions characterized by intense electrical activity for midlatitudes and tropics, respectively. North and South Atlantic were selected to represent regions downwind of $NO_x$ emissions, for mid-latitude and tropic variations, respectively. The highest ranges of $NO_x$ and $O_3$ changes are obtained for continental tropical regions with $\Delta NO_x$ [−33.1; +29.7] ppt and $\Delta O_3$ [−1.56; +2.16] ppb, in January, and $\Delta NO_x$ [−14.3;



+21] ppt and $\Delta O_3$ [−1.18; +1.93] ppb, in July. The largest variation range associated with the tropical continents could be explained by the largest difference on parameter values defining the plume in this region (especially $NO_i$). The smallest intervals are observed over continental mid-latitude regions for winter with $\Delta NO_x$ [−1.7; +1.8] ppt and $\Delta O_3$ [−0.16; +0.72] ppb and over oceanic tropical regions in summer such as $\Delta NO_x$ [−11.5; +2.6] ppt and $\Delta O_3$ [−0.14; +0.92] ppb. As a result, the variability of $NO_x$ and $O_3$ species to the parameter uncertainties is a few ppt for $NO_x$ and less than 2 ppb for $O_3$.

#### 4.3.2 Coefficients related to the nitrification mechanism ($\beta_1$ and $\beta_2$)

In order to estimate the variability of the $NO_x$ and $O_3$ mixing ratios related to the uncertainties on $\beta_1$ and $\beta_2$ fractions (Table 7), the difference between P1 experiment using $\beta_1$ and $\beta_2$ mean values and P1 experiment using minimum and maximum $\beta_1$ and $\beta_2$ coefficients has been calculated. This implies that $\tau$ and $K_{eff}$ are constant.

In January, the highest variability on $NO_x$ mixing ratio is $\Delta NO_x$ [−2.3; +0.9] $\times 10^{-2}$ ppt over continental tropical regions and $\Delta O_3$ [−10; +11] $\times 10^{-4}$ ppb over tropical ocean on $O_3$, while mid-latitude oceanic areas show minimum ranges on $NO_x$ and $O_3$ with $\Delta NO_x \pm 2.3 \times 10^{-2}$ ppt associated with $\Delta O_3$ [−9; +4] $\times 10^{-4}$ ppb. In July, the maximum ranges are calculated over oceans in midlatitudes for $NO_x$ such as $\Delta NO_x$ [−21.1; +6.6] $\times 10^{-2}$ ppt and in tropics for $O_3$ with $\Delta O_3$ [−30; −2] $\times 10^{-4}$ ppb. Finally, the smallest intervals, $\Delta NO_x$ [−0.9; −0.4] $\times 10^{-2}$ ppt and $\Delta O_3$ [−24; −6] $\times 10^{-4}$ ppb, are simulated for tropical ocean and mid-latitude continent, respectively.

In addition, the impact of the nitrification mechanism was assessed comparing the P1 experiment using mean $\beta_1$ and $\beta_2$ values and P2 experiment for which $\beta_1 = \beta_2 = 0$. As a result, taking into account $NO_x$ conversion into $HNO_3$ using the mean $\beta$ fractions calculated in this study does not imply strong changes in $NO_x$ and $O_3$ distributions ($\Delta NO_x < 10^{-4}$ ppb and $\Delta O_3 < 10^{-2}$ ppb).

In the case of significant values of $\beta$ fractions, the rate of the nitrification mechanism should imply a delay of the $O_3$ formation from the $NO_x$ in the plume because of the $NO_x$ storage into $HNO_3$. On the other hand, $HNO_3$ is considered as a one of the main sink for $NO_x$ species undergoing wet deposition and seemingly limiting their affect on global ozone.

The sensitivity tests point out the limited effect of the $NO_x$ conversion to $HNO_3$ within the plume using our $\beta_1$ and $\beta_2$ estimates. The variability on $NO_x$ and $O_3$ mixing ratios related to $\beta$ coefficients is about a few ppt. That could be explained by small $\beta$ values resulting from our estimate unlike Cariolle et al. (2009) highlighted the significant influence of these fractions in the case of aircraft $NO_x$ emissions. In our study, we can easily suppose that the increase of the $\beta_1$ and $\beta_2$ coefficients should be in agreement with the work of Cooper et al. (2014) in reducing the underestimation of $HNO_3$ production induced by $NO_x$ emissions from lightning. Further estimates of $\beta$ should be realized using future observations in cloud anvil of primary species, aerosols and particules needed for $NO_x$ conversion at daytime and nighttime to improve the determination of these parameters. $\beta_1$ coefficient is particularly dependent on the $HO_x$ radicals, which could vary significantly within the cloud anvil in part because of the transport of peroxides from the lower troposphere by convective uplift (Wennberg et al., 1998). Then, the determination of $\beta_2$, corresponding to the $NO_x$ conversion fraction into $HNO_3$ via $N_2O_5$ formation during nighttime is considerably dependent on (i) the estimate of aerosols and ice crystal concentration and their lifetime within the cloud anvil which is highly uncertain according to measurement campaigns and (ii) on the reaction probability on aerosols $\gamma^{\text{aerosol}}_{N_2O_5}$ and ice crystals $\gamma^{\text{ice}}_{N_2O_5}$ from laboratory studies extrapolations.

According to results presented in this section, sensitivity tests show the predominance of the initial NO mixing ratio injected by lightning ($NO_i$) and the diffusion properties of the atmosphere ($D_h$) in the variability of the $NO_x$ and $O_3$ mixing ratios around the mean value in response to the plume-in-grid parameterization in the CTM. In winter, the $NO_x$ and $O_3$ variability is the highest for continental regions in the tropics and the smallest variability is calculated for midlatitudes. In summer, the most important



variability of $NO_x$ and $O_3$ is simulated in tropics over regions characterized by intense $LNO_x$ emissions while the least significant sensitivity is obtained still in the tropics but downwind of emissions (mainly over oceans).

## 5 Conclusions

For the first time, a realistic lightning $NO_x$ chemistry is implemented as a plume parameterization into a global chemical transport model. The key parameters characterizing the lightning-related plume were estimated depending on two main criteria, i.e. the NO mixing ratio injected by lightning ($NO_i$) and the atmospheric diffusion coefficient ($D_h$).

According to the $NO_i$ and $D_h$ ranges, the plume lifetime ($\tau$) and the effective reaction rate constant ($K_{\text{eff}}$) for $NO_x$-$O_3$ chemical interactions were estimated as follow:

- $\tau$ = [0.01; 68.5] h;
- $K_{\text{eff}} = [0.77; 23] \times 10^{-19}$ molecules$^{-1}$ s$^{-1}$ cm$^{-3}$.

Also, for the conditions defined by $NO_i^{\text{mean}}$ and $D_h = 15\,\text{m}^2\,\text{s}^{-1}$:

- $\tau$ is 3 (6) h in midlatitudes and 9 (21.3) h in tropics at daytime (nighttime);
- $K_{\text{eff}}$ is $5.49 \times 10^{-19}$ molecules$^{-1}$ s$^{-1}$ cm$^{-3}$ ($4.55 \times 10^{-19}$ molecules$^{-1}$ s$^{-1}$ cm$^{-3}$) in midlatitudes and $3.64 \times 10^{-19}$ molecules$^{-1}$ s$^{-1}$ cm$^{-3}$ ($2.98 \times 10^{-19}$ molecules$^{-1}$ s$^{-1}$ cm$^{-3}$) in tropics at daytime (nighttime).

Finally, the fractions of $NO_x$ conversion into $HNO_3$ within the plume are $\beta_1 = [1.34; 1.88] \times 10^{-4}$, and $\beta_2 = [0.24; 14.4] \times 10^{-3}$ for day and night conditions respectively.

GEOS-Chem simulations performed using mean value for $NO_i$ and $D_h = 15\,\text{m}^2\,\text{s}^{-1}$ reveal nitrogen species and ozone changes compared to the instantaneous dilution. A decrease of $NO_x$ and $O_3$ mixing ratios at large scale over the regions of strong $LNO_x$ emissions is observed mainly in the Northern Hemisphere in summer and in

the Southern Hemisphere in winter. In the troposphere, maximum decrease of 20 % (6 %) in January and 25 % (8 %) in July for $NO_x$ ($O_3$), are found over Central Africa. In contrast, an increase of $NO_x$ ($O_3$) downwind of emissions is simulated of 20 % (4 %) in January and 18 % (2 %) in July. The $LNO_x$ plume parameterization allows the transport of the effects on the non-linear chemistry occurring within the plume and the conversion of $NO_x$ to the nitrogen reservoir species (mainly $HNO_3$). However, the most significant impact is the transport of the $LNO_x$ as a plume. That implies a delay of (i) the $NO_x$ release into the point grid and (ii) ozone production from $NO_x$ emitted by lightning flashes corresponding to the decrease of the $NO_x$ and $O_3$ mixing ratios at large scale over regions of emissions and their increase over transport pathway.

The variability of the $NO_x$ and $O_3$ mixing ratios around the mean value depending on the known uncertainties on the plume physics and chemistry key parameters has been estimated. The highest sensitivity is obtained for continental tropical regions with $\Delta NO_x$ [−33.1; +29.7] ppt and $\Delta O_3$ [−1.56; +2.16] ppb, in January, and $\Delta NO_x$ [−14.3; +21] ppt and $\Delta O_3$ [−1.18; +1.93] ppb, in July. Concerning $\beta_1$ and $\beta_2$ fractions, the highest variability depending on the fraction uncertainties for $NO_x$ is $\Delta NO_x[-2.3; +0.9] \times 10^{-2}$ ppt over continental tropical regions, and $\Delta O_3$ $[-10; +11] \times 10^{-4}$ ppb for $O_3$ over tropical ocean in January. In summer, the maximum ranges are calculated over oceans in mid-latitudes for $NO_x$ such as $\Delta NO_x[-21.1; +6.6] \times 10^{-2}$ ppt and in tropics for $O_3$ with $\Delta O_3$ $[-30; -2] \times 10^{-4}$ ppb. Accordingly, parameters leading to the highest uncertainties on results and which drive the plume-in-grid parameterization are $NO_i$ and $D_h$.

This study demonstrates the importance to consider the plume-in-grid chemistry related to the lightning $NO_x$ emissions occurring at smaller scale for global calculations. Taking into account the plume dilution into the background atmosphere in time and space with the transport of the $NO_x$ and $O_3$ non-linear chemistry effects and the conversion of $NO_x$ into $HNO_3$ reservoir species, implies more realistic $NO_x$ and $O_3$ concentrations in CTM. The plume-in-grid approach, by allowing realistic sub-grid chemistry will allow improving the different steps in the lightning $NO_x$ emissions modeling such as the convection process, the calculation of the NO molecules produced by lightning



discharges depending on regions according to recent and future satellite observations, and also processes like $HNO_3$ scavenging and $HNO_3$ uptake by ice crystals.

*Acknowledgements.* The GEOS-Chem community (Harvard University) and the Laboratoire d'Aérologie (UPS/CNRS) supported this work. The authors acknowledge for the help of Lee T. Murray (NASA, NY, USA) for his expertise on the lightning $NO_x$ emissions module in the GEOS-Chem model. We thank the University Paul Sabatier III of Toulouse for giving the ATUPS grant allowing the collaboration with the Wolfson Atmospheric Chemistry Laboratories of York in the research group of Mathew J. Evans.

## References

Amos, H. M., Jacob, D. J., Holmes, C. D., Fisher, J. A., Wang, Q., Yantosca, R. M., Corbitt, E. S., Galarneau, E., Rutter, A. P., Gustin, M. S., Steffen, A., Schauer, J. J., Graydon, J. A., Louis, V. L. St., Talbot, R. W., Edgerton, E. S., Zhang, Y., and Sunderland, E. M.: Gas-particle partitioning of atmospheric Hg(II) and its effect on global mercury deposition, Atmos. Chem. Phys., 12, 591–603, doi:10.5194/acp-12-591-2012, 2012. 34096

Aumont, B.: Modélisation de la chimie troposphérique, Université Paris 12 – UFR de Sciences et Technologie, HDR report, Val de Marne, 2005. 34106

Banerjee, A., Archibald, A. T., Maycock, A. C., Telford, P., Abraham, N. L., Yang, X., Braesicke, P., and Pyle, J. A.: Lightning $NO_x$, a key chemistry–climate interaction: impacts of future climate change and consequences for tropospheric oxidising capacity, Atmos. Chem. Phys., 14, 9871–9881, doi:10.5194/acp-14-9871-2014, 2014. 34093

Bechtold, P., Bazile, E., Guichard, F., Mascart, P., and Richard, E.: A mass-flux convection scheme for regional and global models, Q. J. Roy. Meteor. Soc., 127, 869–886, 2000. 34097

Bey, I., Jacob, D. J., Yantosca, R. M., Logan, J. A., Field, B. D., Fiore, A. M., Li, Q., Liu, H. Y., Mickley, L. J., and Schultz, M. G.: Global modeling of tropospheric chemistry with assimilated meteorology: model description and evaluation, J. Geophys. Res., 106, 23073–23095, 2001. 34095, 34096

Bian, H. and Prather, M. J.: Fast-J2: Accurate simulation of stratospheric photolysis in global chemical models, J. Atmos. Chem., 41, 281–296, 2002. 34096

Cariolle, D., Caro, D., Paoli, R., Hauglustaine, D. A., Cuénot, B., Cozic, A., and Paugam, R.: Parametrization of plume chemistry into large-scale atmospheric models: application to

aicraft $NO_x$ emissions, J. Geophys. Res., 114, D19302, doi:10.1029/2009JD011873, 2009. 34098, 34100, 34101, 34102, 34103, 34108, 34121

Choi, Y., Kim, J., Eldering, A., Osterman, G., Yung, Y. L., Gu, Y., and Liou, K. N.: Lightning and anthropogenic $NO_x$ sources over the United States and the western North Atlantic Ocean: impact on OLR and radiative effects, Geophys. Res. Lett., 36, L17806, doi:10.1029/2009GL039381, 2009. 34093

Christian, H. J., Blakeslee, R. J., Boccippio, D. J., Boeck, W. L., Buechler, D. E., Driscoll, K. T., Goodman, S. J., Hall, J. M., Koshak, W. J., Mach, D. M., and Stewart, M. F.: Global frequency and distribution of lightning as observed from space by the Optical Transient Detector, J. Geophys. Res., 108, 4005, doi:10.1029/2002JD002347, 2003. 34093, 34109

Cohard, J.-M. and Pinty, J. P.: A comprehensive two-moment warm microphysical bulk scheme, I: Description and tests, Q. J. Roy. Meteor. Soc., 126, 1815–1842, 2000. 34097

Cooper, M., Martin, R. V., Wespes, C., Coheur, P.-F., Clerbaux, C., and Murray L. T.: Tropospheric nitric acid columns from the IASI satellite instrument interpreted with a chemical transport model: implications for parameterizations of nitric oxide production by lightning, J. Geophys. Res., 119, 10068–10079, 2014. 34094, 34121

Cuxart, J., Bougeault, P., and Redelsperger, J. L.: A turbulence scheme allowing for mesoscale and large-eddy simulations, Q. J. Roy. Meteor. Soc., 126, 1–30, 1999. 34097, 34107

Damian, V., Sandu, A., Damian, M., Potra, F., and Camichael, G. R.: The kinetic preprocessor KPP – a software environment for solving chemical kinectics, Comput. Chem. Eng., 26, 1567–1579, 2002. 34097

Dye, J. E., Ridley, B. A., Skamarock, W., Barth, M., and Venticinque, M.: An overview of the Stratospheric–Tropospheric experiment: radiation, aerosols, and ozone (STERAO)-Deep convection experiment with results for the July 10, 1996 storm, J. Geophys. Res., 105, 10023–10045, 2000. 34101, 34110

Emmerson, K. M. and Evans, M. J.: Comparison of tropospheric gas-phase chemistry schemes for use within global models, Atmos. Chem. Phys., 9, 1831–1845, doi:10.5194/acp-9-1831-2009, 2009. 34097

Evans, M. J. and Jacob, D. J.: Impact of new laboratory studies of $N_2O_5$ hydrolysis on global model budgets of tropospheric nitrogen oxides, ozone, and OH, Geophys. Res. Lett., 32, L09813, doi:10.1029/2005GL022469, 2005. 34112



Gregory, D., Morcrette, J.-J., Jakob, C., Beljaars, A. C. M., and Stockdale, T.: Revision of convection, radiation and cloud schemes in the ECMWF Integrated Forecasting System, Q. J. Roy. Meteor. Soc., 126, 1685–1710, 2000. 34097

Grewe, V.: Impact of climate variability on tropospheric ozone, Sci. Total Environ., 374, 167–181, 2007. 34093

Guenther, A. B., Jiang, X., Heald, C. L., Sakulyanontvittaya, T., Duhl, T., Emmons, L. K., and Wang, X.: The Model of Emissions of Gases and Aerosols from Nature version 2.1 (MEGAN2.1): an extended and updated framework for modeling biogenic emissions, Geosci. Model Dev., 5, 1471–1492, doi:10.5194/gmd-5-1471-2012, 2012. 34096

Hauglustaine, D., Emmons, L., Newchurch, M., Brasseur, G., Takao, T., Matsubara, K., Johnson, J., Ridley, B., Stith, J., and Dye, J.: On the role of lightning $NO_x$ in the formation of tropospheric ozone plumes: a global model perspective, J. Atmos. Chem., 38, 277–294, 2001. 34093

Hauglustaine, D. A., Granier, C., and Brasseur, G. P.: Impact of present aircraft emissions of nitrogen oxides on troposheric ozone and climate forcing, Geophys. Res. Lett., 21, 2031–2034, 1994. 34093

Hudman, R.C., Jacob, D. J., Turquety, S., Leibensperger, E. M., Murray, L. T., Wu, S., Gilliland, A. B., Avery, M., Bertram, T. H., Brune, W., Coben, R. C., Dibb, J. E., Flocke, F. M., Fried, A., Holloway, J., Neumann, J. A., Orville, R., Perning, A., Ren, X., Sachse, G. W., Singh, H. B., Swanson, A., and Wooldridge, P. J.: Surface and lightning sources of nitrogen oxides over the United States: magnitudes, chemical evolution, and outflow, J. Geophys. Res., 112, D12S05, doi:10.1029/2006JD007912, 2007. 34093, 34094

Huntrieser, H., Schlager, H., Feigl, C., and Höller, H.: Transport and production of $NO_x$ in electrified thunderstorms: survey of previous studies and new observations at midlatitudes, J. Geophys. Res., 103, 28247–28264, 1998. 34110

Huntrieser, H., Feigl, C., Schlager, H., Schröder, F., Gerbig, C., and van Velthoven, P.: Airborne measurements of $NO_x$, tracer species, and small particles during the European Lightning Nitrogen Oxides Experiment, J. Geophys. Res., 107, 4113, doi:10.1029/2000JD000209, 2002. 34101, 34110, 34112

Huszar, P., Cariolle, D., Paoli, R., Halenka, T., Belda, M., Schlager, H., Miksovsky, J., and Pisoft, P.: Modeling the regional impact of ship emissions on $NO_x$ and ozone levels over the Eastern Atlantic and Western Europe using ship plume parameterization, Atmos. Chem. Phys., 10, 6645–6660, doi:10.5194/acp-10-6645-2010, 2010. 34094, 34098

Jacobson, M. Z. and Turco, R. P.: SMVGEAR: a sparse-matrix, vectorized gear code for atmospheric models, Atmos. Environ., 28, 273–284, 1994. 34096
Jaeglé, L., Jacob, D. J., Brune, W. H., Tan, D., Faloona, I. C., Weinheimer, A. J., Ridley, B. A., Campos, T. L., and Sachse, G. W.: Soucres and chemistry of $NO_x$ in the upper troposphere over the United Sates, Geophys. Res. Lett., 25, 1705–1708, 1998. 34101
Jenkin, M. E., Saunders, S. M., and Pilling, M. J.: The tropospheric degradation of volatile organic compounds: a protocol for mechanism development, Atmos. Environ., 31, 81–104, 1997. 34097
Klemp, J. B. and Wilhelmson, R. B.: The simulation of three-dimensional convective storm dynamics, J. Atmos. Sci., 35, 1070–1096, 1978. 34107
Knollenberg, R. G.: Measurements of the growth of the ice budget in a persisting contrail, J. Atmos. Sci., 29, 1367–1374, 1972. 34108
Knollenberg, R. G., Kelly, K., and Wilson, J. C.: Measurements of high number densities of ice crystals in the tops of tropical cumulonimbus, J. Geophys. Res., 98, 8639–8664, 1993. 34112
Labrador, L. J., von Kuhlmann, R., and Lawrence, M. G.: Strong sensitivity of the global mean OH concentration and te tropospheric oxidizing efficiency to the source of $NO_x$ from lightning, Geophys. Res. Lett., 31, L06102, doi:10.1029/2003GL019229, 2004. 34093
Lafore, J. P., Stein, J., Asencio, N., Bougeault, P., Ducrocq, V., Duron, J., Fischer, C., Héreil, P., Mascart, P., Masson, V., Pinty, J. P., Redelsperger, J. L., Richard, E., and Vilà-Guerau de Arellano, J.: The Meso-NH Atmospheric Simulation System. Part I: adiabatic formulation and control simulations, Ann. Geophys., 16, 90–109, doi:10.1007/s00585-997-0090-6, 1998. 34097
Lange, L., Hoor, P., Helas, G., Fischer, H., Brunner, D., Scheeren, B., Williams, J., Wong, S., Wohlfrom, K.-H., Arnold, F., Ström, J., Krejci, R., Lelieveld, J., and Andreae, M. O.: Detection of lightning-produced NO in the midlatitude upper troposphere during STREAM 1998, J. Geophys. Res., 106, 27777–27785, 2001. 34110
Lascaux, F., Richard, E., and Pinty, J. P.: Numerical simulations of three different MAP IOPs and the associated microphysical processes, Q. J. Roy. Meteor. Soc., 132, 1907–1926, 2006. 34097
Lin, J.-T. and McElroy, M. B.: Impacts of boundary layer mixing on pollutant vertical profiles in the lower troposphere: implications to satellite remote sensing, Atmos. Environ., 44, 1726–1739, 2010. 34096



Lin, S.-J. and Rood, R. B.: Multidimensional flux-form semi-lagrangian transport scheme, Mon. Weather Rev., 124, 2046–2070, 1996. 34096
Lin, X., Trainer, M., and Liu, S. C.: On the nonlinearity of the tropospheric ozone production, J. Geophys. Res., 93, 15879–15888, 1988. 34094
Liu, H., Jacob, D. J., Rey, I., and Yantosca, R. M.: Constraints from $^{210}$Pb and $^{7}$Be on wet deposition and transport in a global three-dimensional chemical tracer model driven by assimilated meteorological fields, J. Geophys. Res., 106, 12109–12128, 2001. 34096
Lobert, J. M., Keene, W. C., Logan, J. A., and Yevich, R.: Global chlorine emissions from biomass burning: reactive chlorine emissions inventory, J. Geophys. Res., 104, 8373–8389, 1999. 34096
Madronich, S. and Flocke, S.: Environmental Photochemistry, Springer Berlin Heidelberg, Germany, ISBN: 9783662147351, doi:10.1007/978-3-540-69044-3, 1999. 34097
Martin, R. V., Jacob, D. J., Logan, J. A., Bey, I., Yantosca, R. M., Staudt, A. C., Li, Q., Fiore, A. M., Duncan, B. N., and Liu, H.: Interpretation of TOMS observations of tropical tropospheric ozone with a global model and in situ observations, J. Geophys. Res., 107, 4351, doi:10.1029/2001JD001480, 2002. 34096
Martin, R. V., Sauvage, B., Folkins, I., Sioris, C. E., Boone, C., Bernath, P., and Ziemke, J.: Space-based constraints on the production of nitric oxide by lightning, J. Geophys. Res., 112, D09309, doi:10.1029/2006JD007831, 2007. 34093, 34094, 34097
Monks, P. S.: Gas-phase radical chemistry in the tropopshere, Chem. Soc. Rev., 34, 376–395, 2005. 34105
Moorthi, S. and Suarez, M. J.: Relaxed Arakawa-Schubert: a parameterization of moist convection for general circulation models, Mon. Weather Rev., 120, 978–1002, 1991. 34096
Murray, L. T., Jacob, D. J., Logan, J. A., Hudman, R. C., and Koshak, J.: Optimized regional and interannual variability of lightning in a global chemical transport model constrained by LIS/OTD satelite data, J. Geophys. Res., 117, D20307, doi:10.1029/2012JD017934, 2012. 34093, 34097
Olivier, J. G. J.: Recent trends in global greenhouse gas emissions: regional trends and spatial distribution of key sources, Environment Sciences, 2, 81–89, 2005. 34096
Ott, L. E., Pickering, K. E., Stenchikov, G. L., Allen, D. J., DeCaria, A. J., Ridley, B., Lin, R. F., Lang, S., and Tao, W.-K.: Production of lightning $NO_x$ and its vertical distribution calculated from three-dimensional cloud-scale chemical transport model simulations, J. Geophys. Res., 115, D04301, doi:10.1029/2009JD011880, 2010. 34096, 34100

Paoli, R., Cariolle, D., and Sausen, R.: Review of effective emissions modeling and computation, Geosci. Model Dev., 4, 643–667, doi:10.5194/gmd-4-643-2011, 2011. 34098
Pickering, K. E., Thompson, A. M., Dickerson, R. R., Luke, W. T., MacNamara, D. P., Greenberg, J. P., and Zimmerman, P. R.: Model calculations of tropospheric ozone production potentiel following observed convective events, J. Geophys. Res., 95, 14049–14062, 1990. 34093
Pickering, K. E., Wang, Y., Tao, W.-K., Price, C., and Müller, J.-F.: Vertical distributions of lightning $NO_x$ for use in regional and global chemical transport models, J. Geophys. Res., 103, 31203–31216, 1998. 34094, 34096
Pinty, J. P. and Jabouille, P.: A mixed-phase cloud parameterization for use in a mesoscale non-hydrostatic model: simulations of a squall line and of orographic precipitation, American Meteorological Society, Conference on cloud physics, 17–21 August 1998, Everett, WA, USA, 217–220, 1999. 34097
Price, C. and Rind, D.: A simple lightning parameterization for calculating global lightning distributions, J. Geophys. Res., 97, 9919–9933, 1992. 34093, 34096
Price, C. and Rind, D.: Possible implications of global climate change on global lightning distributions and frequencies, J. Geophys. Res., 99, 10823–10831, 1994. 34096
Sander, S. P., Friedl, R. R., Golden, D. M., Kurylo, M. J., Moortgat, G. K., Wine P. H., Ravishankara, A. R., Kolb, C. E., Molina, M. J., Finlayson-Pitts, B. J., Huie, R. E., and Orkin, V. L.: Chemical Kinetics and Photochemical Data for Use in Atmosperic Studies, Evaluation Number 15, Tech. rep., NASA, Jet Propulsion Laboratory, California Institute of Technology, Pasadena, California, USA, 2006. 34112
Saunders, S. M., Jenkin, M. E., Derwent, R. G., and Pilling, M. J.: Protocol for the development of the Master Chemical Mechanism, MCM v3 (Part A): tropospheric degradation of non-aromatic volatile organic compounds, Atmos. Chem. Phys., 3, 161–180, doi:10.5194/acp-3-161-2003, 2003. 34098
Sauvage, B., Martin, R. V., van Donkelaa, A., and Ziemke, J. R.: Quantification of the factors controlling tropical tropopsheric ozone and the South Atlantic maximum, J. Geophys. Res., 112, D11309, doi:10.1029/2006JD008008, 2007a. 34093
Sauvage, B., Martin, R. V., van Donkelaar, A., Liu, X., Chance, K., Jaeglé, L., Palmer, P. I., Wu, S., and Fu, T.-M.: Remote sensed and in situ constraints on processes affecting tropical tropospheric ozone, Atmos. Chem. Phys., 7, 815–838, doi:10.5194/acp-7-815-2007, 2007b. 34093, 34096





Schumann, U. and Huntrieser, H.: The global lightning-induced nitrogen oxides source, Atmos. Chem. Phys., 7, 3823–3907, doi:10.5194/acp-7-3823-2007, 2007. 34093
Stith, J., Dye, J., Ridley, B., Laroche, P., Defer, E., Hübler, G., Zerr, R., and Venticinque, M.: NO signatures from lightning flashes, J. Geophys. Res., 104, 16081–16089, 1999. 34110
Stockwell, D. Z., Giannakopoulos, C., Plantevin, P. H., Carver, G. D., Chipperfield, M. P., Law, K. S., Pyle, J. A., Shallcross, D. E., and Wang, K. Y.: Modelling $NO_x$ from lightning and its impact on global chemical fields, Atmos. Environ., 33, 4477–4493, 1999. 34093
Streets, D. G., Zhang, Q., Wang, L., He, K., Hao, J., Wu, Y., Tang, Y., and Carmichael, G. R.: Revisting China's CO emissions after the Transport and Chemical evolution over the Pacific (TRACE-P) mission: synthesis of inventories, atmospheric modeling, and observations, J. Geophys. Res., 111, D14306, doi:10.1029/2006JD007118, 2006. 34096
Tost, H., Jöckel, P., and Lelieveld, J.: Lightning and convection parameterisations – uncertainties in global modelling, Atmos. Chem. Phys., 7, 4553–4568, doi:10.5194/acp-7-4553-2007, 2007. 34093
Trier, S. B. and Sharman, R. D.: Convection-permitting simulations of the environment supporting widespread turbulence within the upper-level outflow of a mesoscale convective system, American Meteorological Society, 137, 1972–1990, 2008. 34107
Tulet, P., Crassier, V., Solmon, F., Guedalia, D., and Rosset, R.: Description of the mesoscale nonhydrostatic chemistry model and application to a transboundary pollution episode between northern France and southern England, J. Geophys. Res., 108, 4021, doi:10.1029/2000JD000301, 2003. 34097
Tulet, P., Grini, A., Griffin, R. J., and Petitcol, S.: ORILAM-SOA: A compitationnaly efficient model for predicting secondary organic aerosols in three-dimensional atmospheric models, J. Geophys. Res., 111, D23208, doi:10.1029/2006JD007152, 2006. 34097
Wang, Q., Jacob, D. J., Fisher, J. A., Mao, J., Leibensperger, E. M., Carouge, C. C., Le Sager, P., Kondo, Y., Jimenez, J. L., Cubison, M. J., and Doherty, S. J.: Sources of carbonaceous aerosols and deposited black carbon in the Arctic in winter-spring: implications for radiative forcing, Atmos. Chem. Phys., 11, 12453–12473, doi:10.5194/acp-11-12453-2011, 2011. 34096
Wang, Y., Jacob, D. J., and Logan, J. A.: Global simulation of tropospheric $O_3$-$NO_x$-hydrocarbon chemistry – 1. Model formulation, J. Geophys. Res., 103, 10713–10725, 1998. 34096
Weiss, S. A., MacGorman, D. R., and Calhoun, K. M.: Lightning in the anvils of supercell thunderstorms, Mon. Weather Rev., 140, 2064–2079, 2012. 34093

Wennberg, P. O., Hanisco, T. F., Jaeglé, L., Jacob, D. J., Hintsa, E. J., Lanzendorf, E. J., Anderson, J. G., Gao, R.-S., Keim, E. R., Donnelly, S. G., Del Negro, L. A., Fahey, D. W., McKeen, S. A., Salawitch, R. J., Webster, C. R., May, R. D., Herman, R. L., Proffitt, M. H., Margitan, J. J., Atlas, E. L., Schauffer, S. M., Flocke, F., McElroy, C. T., and Bui, T. P.: Hydrogen radicals, nitrogen radicals and the production of $O_3$ in the upper troposphere, Science, 279, 49–53, doi:10.1126/science.279.5347.49, 1998. 34121

Wesely, M. L.: Parameterization of surface resistances to gaseous dry deposition in regional-scale numerical models, Atmos. Environ., 23, 1293–1304, 1989. 34096

WMO: Scientific Assessment of Ozone Depletion: 1998, Tech. rep., World Meteorological Organization, Geneva, Switzerland, 1999. 34093

Yevich, R. and Logan, J. A.: An assessment of biofuel use and burning of agricultural waste in the developing world, Global Biogeochem. Cy., 17, 1095, doi:10.1029/2002GB001952, 2003. 34096

Yienger, J. J. and Levy, H.: Empirical model of global soil-biogenic $NO_x$ emissions, J. Geophys. Res., 100, 11447–11464, 1995. 34096

Zhang, Q., Streets, D. G., Carmichael, G. R., He, K. B., Huo, H., Kannari, A., Klimont, Z., Park, I. S., Reddy, S., Fu, J. S., Chen, D., Duan, L., Lei, Y., Wang, L. T., and Yao, Z. L.: Asian emissions in 2006 for the NASA INTEX-B mission, Atmos. Chem. Phys., 9, 5131–5153, doi:10.5194/acp-9-5131-2009, 2009. 34096

Zhang, R., Tie, X., and Bond, D. W.: Impacts of anthropogenic and natural $NO_x$ sources over the U. S. on tropospheric chemistry, P. Natl. Acad. Sci. USA, 100, 1505–1509, 2003. 34093



**Table 1.** The initial atmospheric parameters and background concentrations of chemical species from GEOS-Chem outputs for the DSMACC chemical box model simulations.

| | TEMP | PRESS | $O_3$ | NO | $NO_2$ | $HNO_3$ | $HNO_4$ | PAN | $N_2O_5$ | CO |
|---|---|---|---|---|---|---|---|---|---|---|
| Units | (K) | (hPa) | (ppb) | (ppb) | (ppb) | (ppb) | (ppb) | (ppb) | (ppt) | (ppb) |
| Midlatitudes | 228 | 313 | 67 | 0.04 | 0.01 | 0.15 | 0.02 | 0.1 | 2 | 94 |
| Tropics | 240 | 313 | 26 | 0.03 | 0.003 | 0.02 | 0.006 | 0.03 | 2.3 | 93 |

| Units | OH (ppb) | $HO_2$ (ppt) | $H_2O_2$ (ppt) | $CH_2O$ (ppb) | $CH_4O_2$ (ppb) | $C_3H_8$ (ppb) | $C_5H_8$ (ppb) | $C_2H_4O$ (ppb) | $C_3H_6O$ (ppb) |
|---|---|---|---|---|---|---|---|---|---|
| Midlatitudes | 0.2 | 4 | 0.4 | 0.06 | 0.1 | 0.47 | 0 | 7.5 | 4 |
| Tropics | 0.06 | 6 | 0.34 | 0.03 | 0.17 | 0.13 | 7.5 | 7.5 | 4 |

**Table 2.** The plume lifetime $\tau$ (h) calculated for midlatitudes and tropics depending on the initial NO mixing ratio injected by lightning emissions ($NO_i$, ppb) and the horizontal diffusion coefficient ($D_h$, $m^2 s^{-1}$) for day (upper table) and night conditions (bottom table).

| | Day | | | | | |
|---|---|---|---|---|---|---|
| $\tau$ (h) | Midlatitudes | | | Tropics | | |
| $NO_i$ (ppb) | 0.7 | 3.4 | 10 | 2.8 | 10 | 29.7 |
| $D_h = 0.1$ ($m^2 s^{-1}$) | 1.55 | 8.14 | 23.9 | 4.40 | 23.1 | 67.9 |
| $D_h = 15$ ($m^2 s^{-1}$) | 0.1 | 3.17 | 18.6 | 0.27 | 8.90 | 52.8 |
| $D_h = 100$ ($m^2 s^{-1}$) | 0.01 | 0.47 | 4.17 | 0.04 | 1.32 | 11.7 |
| | Night | | | | | |
| $\tau$ (h) | Midlatitudes | | | Tropics | | |
| $NO_i$ (ppb) | 0.7 | 3.4 | 10 | 2.8 | 10 | 29.7 |
| $D_h = 0.1$ ($m^2 s^{-1}$) | 1.62 | 8.19 | 24.1 | 4.74 | 23.4 | 68.5 |
| $D_h = 15$ ($m^2 s^{-1}$) | 0.31 | 6.19 | 22 | 2.77 | 21.3 | 66.4 |
| $D_h = 100$ ($m^2 s^{-1}$) | 0.05 | 1.23 | 10.6 | 0.43 | 10.5 | 55.4 |



**Table 3.** The effective reaction rate constant $K_{eff}$ ($10^{-19}$ molecules$^{-1}$ s$^{-1}$ cm$^{-3}$) in midlatitudes and tropics depending on the initial NO mixing ratio injected by lightning emissions ($NO_i$, ppb) and the horizontal diffusion coefficient ($D_h$, $m^2 s^{-1}$) for day (upper table) and night conditions (bottom table).

| | Day | | | | | |
|---|---|---|---|---|---|---|
| $K_{eff}$ ($10^{-19}$ molecules$^{-1}$ s$^{-1}$ cm$^{-3}$) | Midlatitudes | | | Tropics | | |
| $NO_i$ (ppb) | 0.7 | 3.4 | 10 | 2.8 | 10 | 29.7 |
| $D_h = 0.1$ ($m^2 s^{-1}$) | 1.28 | 1.24 | 1.51 | 0.77 | 1.2 | 1.83 |
| $D_h = 15$ ($m^2 s^{-1}$) | 8.44 | 5.49 | 5.43 | 7.79 | 3.64 | 4.13 |
| $D_h = 100$ ($m^2 s^{-1}$) | 12.1 | 16.4 | 14.4 | 23 | 19.8 | 13 |
| | Night | | | | | |
| $K_{eff}$ ($10^{-19}$molecules$^{-1}$ s$^{-1}$ cm$^{-3}$) | Midlatitudes | | | Tropics | | |
| $NO_i$ (ppb) | 0.7 | 3.4 | 10 | 2.8 | 10 | 29.7 |
| $D_h = 0.1$ ($m^2 s^{-1}$) | 1.28 | 1.24 | 1.51 | 0.77 | 1.10 | 1.83 |
| $D_h = 15$ ($m^2 s^{-1}$) | 4.84 | 4.55 | 5.43 | 2.3 | 2.98 | 4.13 |
| $D_h = 100$ ($m^2 s^{-1}$) | 7.36 | 8.39 | 6.73 | 6.45 | 3.94 | 5.16 |

**Table 4.** The fractions of $NO_x$ conversion into $HNO_3$ within the plume ($\beta_1$ and $\beta_2$) in midlatitudes and tropics depending on the initial NO mixing ratio injected by lightning emissions ($NO_i$, ppb) and on particles for day (upper table) and night conditions (bottom table).

| | Day | | | | | |
|---|---|---|---|---|---|---|
| $\beta_1$ ($10^{-4}$) | Midlatitudes | | | Tropics | | |
| $NO_i$ (ppb) | 0.7 | 3.4 | 10 | 2.8 | 10 | 29.7 |
| Aerosols | 2.53 | 3.34 | 3.45 | 2.51 | 2.95 | 2.6 |
| Ice | 0.23 | 0.3 | 0.3 | 0.2 | 0.23 | 0.3 |
| Mean | 1.38 | 1.8 | 1.88 | 1.34 | 1.59 | 1.47 |
| | Night | | | | | |
| $\beta_2$ ($10^{-3}$) | Midlatitudes | | | Tropics | | |
| $NO_i$ (ppb) | 0.7 | 3.4 | 10 | 2.8 | 10 | 29.7 |
| Aerosols | 14.3 | 9.89 | 8 | 4.9 | 1.69 | 0.24 |
| Ice | 14.4 | 9.96 | 8.06 | 4.89 | 1.70 | 0.24 |
| Mean | 14.4 | 9.92 | 8.03 | 4.88 | 1.7 | 0.24 |



**Table 5.** Values of the parameters for the plume parameterization corresponding to the experiments P1 and P2.

| Parameters | Experiments | | | | | | | | | | | | |
|---|---|---|---|---|---|---|---|---|---|---|---|---|---|
| | P1 | | | | | | | | | P2 | | | |
| $D_h$ ($m^2 s^{-1}$) | 0.1 | | | 15 | | | 100 | | | 15 | | | |
| $NO_i$ (ppb) | Min | Mean | Max | Min | Mean | Max | Min | Mean | Max | Mean | | | |
| Midlatitudes | 0.7 | 3.4 | 10 | 0.7 | 3.4 | 10 | 0.7 | 3.4 | 10 | 3.4 | | | |
| Tropics | 2.8 | 10.2 | 29.7 | 2.8 | 10.2 | 29.7 | 2.8 | 10.2 | 29.7 | 10.2 | | | |
| $\beta_1$ | | | | | Mean | | | | | 0 | Min | Mean | Max |
| $\beta_2$ | | | | | Mean | | | | | 0 | Min | Mean | Max |

**Table 6.** The variability of $NO_x$ (in ppt) and $O_3$ (in ppb) depending on the horizontal diffusion coefficient ($D_h$, $m^2 s^{-1}$) and on the $NO_i$ mixing ratio (ppb) injected by lightning for midlatitudes (Florida and North Atlantic) and tropics (Congo and South Atlantic) in January and July.

| | January | | | | July | | | |
|---|---|---|---|---|---|---|---|---|
| | Midlatitudes | | Tropics | | Midlatitudes | | Tropics | |
| | Florida | North Atlantic | Congo | South Atlantic | Florida | North Atlantic | Congo | South Atlantic |
| $\Delta NO_x \pm$ | [−1.7; +1.8] | [−8.2; +1.7] | [−33.1; +29.7] | [−6.5; +6.9] | [−9.3; +5.4] | [−21.1; +6.6] | [−14.3; +21] | [−11.5; +2.6] |
| $\Delta O_3 \pm$ | [−0.16; +0.72] | [−0.12; +0.53] | [−1.56; +2.16] | [−0.49; +0.94] | [−0.44; +1.01] | [−0.49; +0.66] | [−1.18; +1.93] | [−0.14; +0.92] |





**Table 7.** The variability of $NO_x$ (in ppt, $\times 10^{-2}$) and $O_3$ (in ppb, $\times 10^{-4}$) depending on $\beta_1$ and $\beta_2$ values for midlatitudes (Florida and North Atlantic) and tropics (Congo and South Atlantic) in January and July. Experiment P1, using $D_h = 15\,m^2 s^{-1}$ and $NO_i^{mean}$, performed with the GEOS-Chem model.

| | January | | | | July | | | |
|---|---|---|---|---|---|---|---|---|
| | Midlatitudes | | Tropics | | Midlatitudes | | Tropics | |
| | Florida | North Atlantic | Congo | South Atlantic | Florida | North Atlantic | Congo | South Atlantic |
| $\Delta NO_x \pm$ | [−1.6; −0.06] | [−2.3; −2.3] | [−2.3; +0.9] | [+0.3; +0.6] | [−3.3; +1.4] | [−21.1; +6.6] | [+0.4; +2.1] | [−0.9; −0.4] |
| $\Delta O_3 \pm$ | [−9; +5] | [−9; +4] | [−3; +22] | [−10; +11] | [−24; −6] | [−6; +19] | [−8; +17] | [−30; −2] |

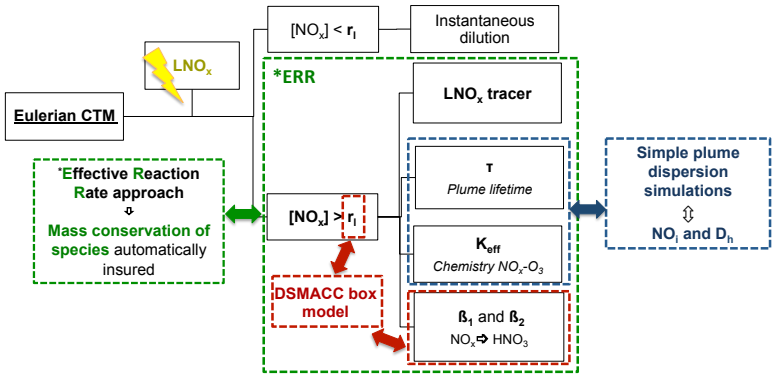


**Figure 1.** The lightning $NO_x$ plume parameterization based on the Effective Reaction Rate approach.





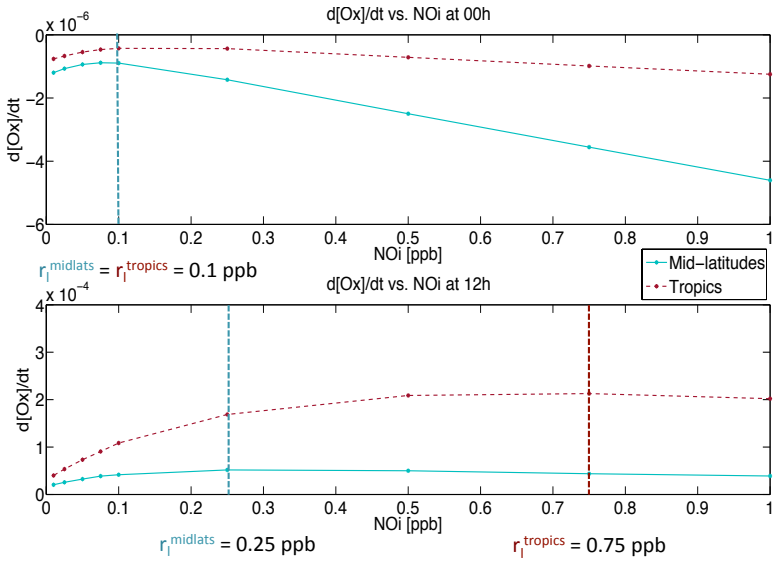


**Figure 2.** $r_l$ critical value and odd oxygen trends from DSMACC chemistry box model simulations for midlatitudes (solid line) and tropics (dotted line) **(a)** at midnight (upper panel) and **(b)** at midday (bottom panel).

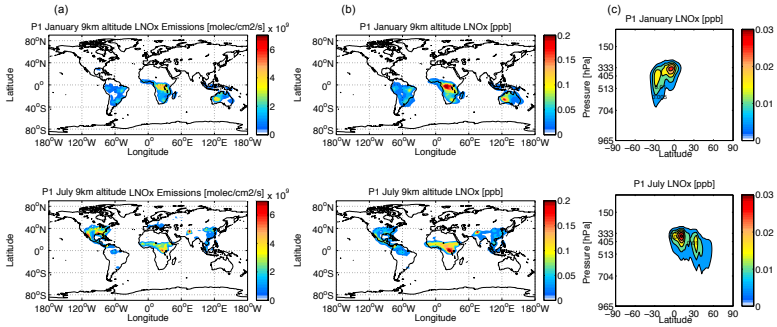


**Figure 3.** (left panels, **a**) Geographical distributions at 9 km altitude of lightning $NO_x$ emissions, (middle panels, **b**) the geographical distributions of the related $LNO_x$ tracer (in ppb) and (right panels, **c**) the zonal averaged of the $LNO_x$ tracer (in ppb), for January (top) and July (bottom). Experiment P1, using $D_h = 15\,m^2\,s^{-1}$ and $NO_i^{mean}$, performed with the GEOS-Chem model.





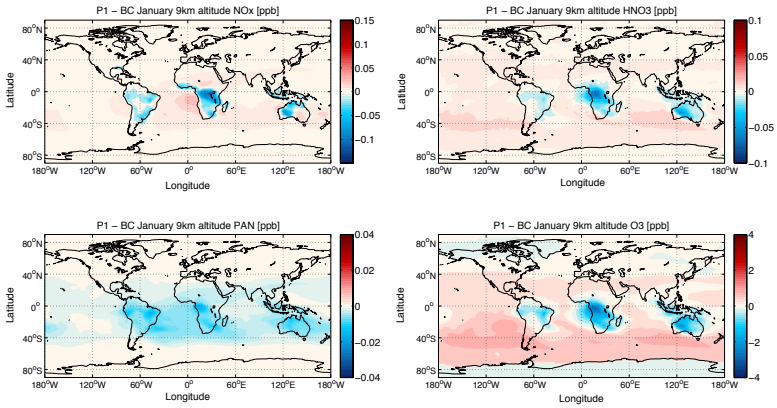


**Figure 4.** Geographical distributions of $NO_x$, $HNO_3$, PAN, and $O_3$ variations (in ppb) at 9 km altitude for January from the absolute difference between P1 and BC experiments. P1 was performed using $D_h = 15\,m^2\,s^{-1}$ and $NO_i^{mean}$ with GEOS-Chem.

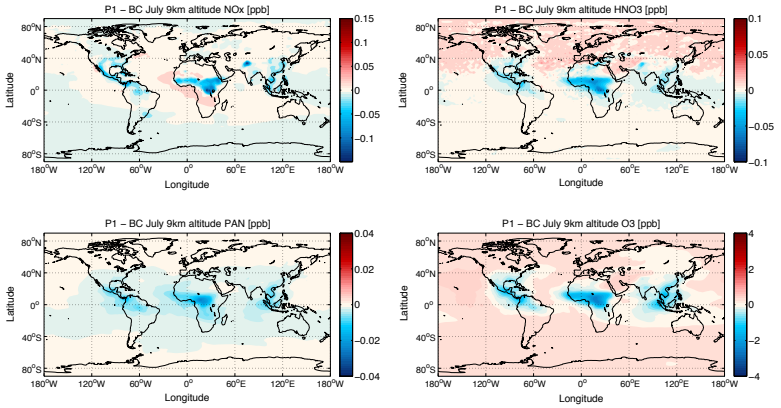


**Figure 5.** Geographical distributions of $NO_x$, $HNO_3$, PAN, and $O_3$ variations (in ppb) at 9 km altitude for July from the absolute difference between P1 and BC experiments. P1 was performed using $D_h = 15\,m^2\,s^{-1}$ and $NO_i^{mean}$ with GEOS-Chem.





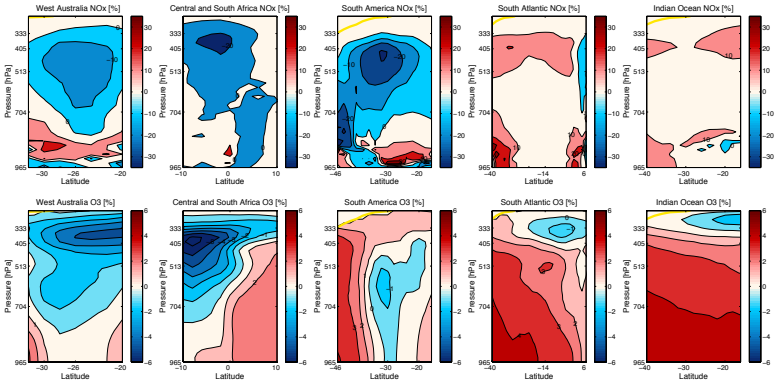


**Figure 6.** Zonal averaged $NO_x$ (upper panels) and $O_3$ (bottom panels) variations (in %) over the regions characterized by strong $NO_x$ emissions for January (the yellow solid line represents the tropopause level), from the relative difference between P1 and BC experiments ((P1–BC) /BC). P1 was performed using $D_h = 15\,m^2\,s^{-1}$ and $NO_i^{mean}$ with GEOS-Chem.

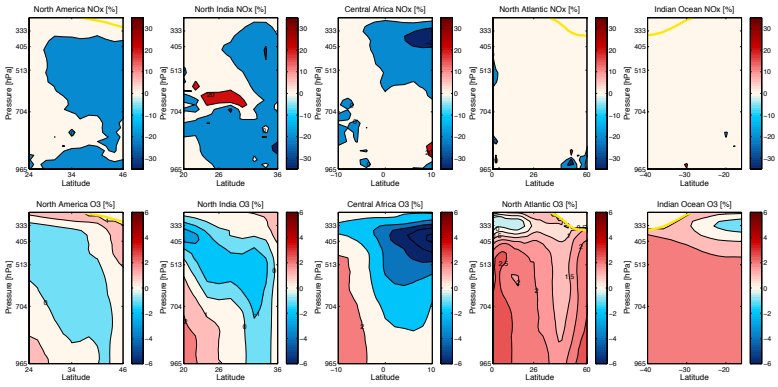


**Figure 7.** Zonal averaged $NO_x$ (upper panels) and $O_3$ (bottom panels) variations (in %) over the regions characterized by strong $NO_x$ emissions for July (the yellow solid line represents the tropopause level), from the relative difference between P1 and BC experiments ((P1–BC) /BC). P1 was performed using $D_h = 15\,m^2\,s^{-1}$ and $NO_i^{mean}$ with GEOS-Chem.





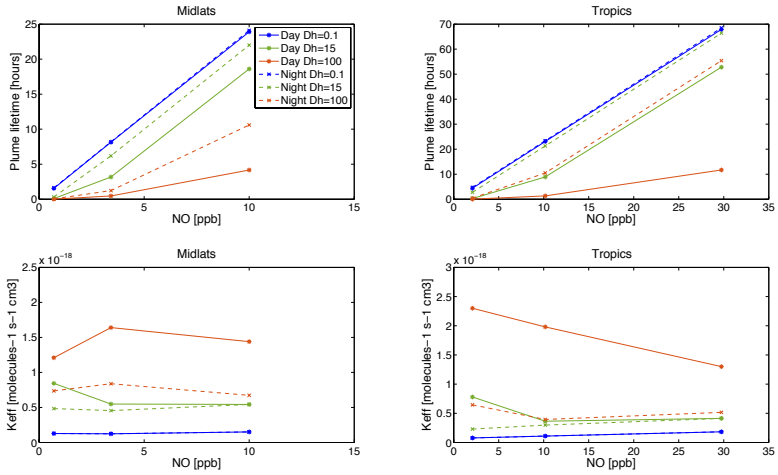


**Figure 8.** The plume lifetime ($\tau$, upper panels) and the effective reaction rate constant ($K_{eff}$, bottom panels) depending (i) on the horizontal coefficient diffusion ($D_h$, $m^2\,s^{-1}$) for midlatitudes (left panels) and tropics (right panels) and (ii) on the NO mixing ratio injected by lightning ($NO_i$, in ppb).

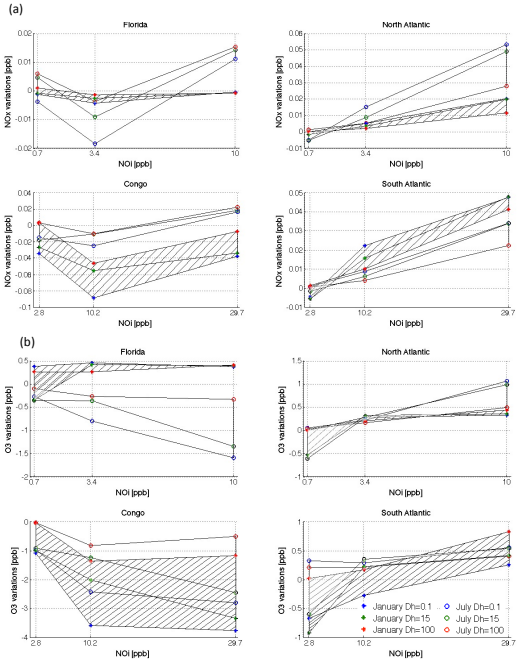


**Figure 9.** The $NO_x$ **(a)** and $O_3$ **(b)** variability at 9 km altitude depending on the horizontal coefficient diffusion ($D_h$, $m^2 s^{-1}$) and on the NO mixing ratio injected by lightning ($NO_i$, ppb) for midlatitudes (Florida and North Atlantic) and tropics (Congo and South Atlantic). Intervals are hatched in January and non-hatched in July. Markers correspond to the $NO_x$ variations simulated for $D_h = 0.1\,m^2 s^{-1}$ (red ones), $D_h = 15\,m^2 s^{-1}$ (blue ones) and $D_h = 100\,m^2 s^{-1}$ (green ones).